## General Disclaimer

## One or more of the Following Statements may affect this Document

- This document has been reproduced from the best copy furnished by the organizational source. It is being released in the interest of making available as much information as possible.

- This document may contain data, which exceeds the sheet parameters. It was furnished in this condition by the organizational source and is the best copy available.

- This document may contain tone-on-tone or color graphs, charts and/or pictures, which have been reproduced in black and white.

- This document is paginated as submitted by the original source.

- Portions of this document are not fully legible due to the historical nature of some of the material. However, it is the best reproduction available from the original submission.

Produced by the NASA Center for Aerospace Information (CASI)

JUL 1983
RECEIVED
NASA STI FACILITY
ACCESS DEPT.

NASA

Technical Memorandum 85034

# HIGH ENERGY ASTROPHYSICS LABORATORY CONTRIBUTIONS TO THE 18th INTERNATIONAL COSMIC RAY CONFERENCE AUGUST 22 TO SEPTEMBER 3, 1983

(NASA-TM-85034) HIGH ENERGY ASTROPHYSICS LABORATORY CONTRIBUTIONS TO THE 18TH INTERNATIONAL COSMIC RAY CONFERENCE (NASA) 53 p HC A04/MF A01 CSCL 03B
N83-30351
Unclas
G3/93 28152

MAY 1983

National Aeronautics and
Space Administration

**Goddard Space Flight Center**
Greenbelt, Maryland 20771

Contents


| Contents | Designation |
|---|---|
| "Gamma-Ray Burst High Time-Resolution Spectral Observations Made with the Solar Maximum Mission" U.D. Desai, J.P. Norris, T.L. Cline, B.R. Dennis and K.J.Frost | XG2-2 |
| "Diffuse Galactic Emission of High Energy Gamma Rays" D.A. Kniffen, C.E. Fichtel, and R.C. Hartman | XG5-4 |
| "Electron Propagation in the Leaky Box Model with a Truncated Pathlength Distribution" B.G. Mauger and J.F. Ormes | OG3-5 |
| "Local Superbubble Model of Cosmic Ray Propagation" R.E. Streitmatter, V.K. Balasubrahmanyan, J.F. Ormes, and R.J. Protheroe | OG5.1-9 |
| "On the Localized Nature of the Galactic Cosmic Rays" J.F. Ormes | OG5.1-10 |
| "Acceleration and Propagation of Galactic Cosmic Rays: Implications of HEAO-3 Data" J.F. Ormes and R.J. Protheroe | OG5.2-14 |
| "How Do Cosmic Rays Change Their Energy in the Solar Wind? Frank C. Jones | MG1-3 |
| "Solar $^3$He-Rich Events Observed on ISEE-3" D.V. Reames and T.T. von Rosenvinge | SP-2 |
| "Solar Flare Neutrons and Gamma Ray Lines" R.E. Lingenfelter, R. Ramaty, R.J. Murphy, and B. Kozlovsky | SP3-10 |
| "The GSFC Advanced Compton Telescope (ACT) R. Hartman, C. Fichtel, D. Kniffen, G. Stacy, and J. Trombka | T1-8 |
| "EGRET: The High Energy Gamma Ray Telescope for NASA's Gamma Ray Observatory" C.E. Fichtel, D.L. Bertsch, R.C. Hartman, D.A. Kniffen, D.J. Thompson, R. Hofstadter, E.B. Hughes, L.E. Campbell-Finman, K. Pinkau, H. Mayer-Hasselwander, G. Kanbach, H. Rothermel, M. Sommer, A.J. Favale, and E.J. Schneid | T1-10 |
| "A Large Area Experiment to Determine Cosmic Ray Isotopic Abundances" B.G. Mauger, V.K. Balasubrahmanyan, J.F. Ormes, R.E. Streitmatter, W. Heinrich, M. Simon, and H.O. Tittel | T2-1 |
| "A Method to Detect Ultra High Energy Electrons Using Earth's Magnetic Field as a Radiator" S.A. Stephens and V.K. Balasubrahmanyan | T2-22 |

# GAMMA-RAY BURST HIGH TIME-RESOLUTION SPECTRAL OBSERVATIONS MADE WITH THE SOLAR MAXIMUM MISSION

U. D. Desai, J. P. Norris*, T. L. Cline, B. R. Dennis, K. J. Frost
NASA/Goddard Space Flight Center
Greenbelt, MD 20771, USA

Results from the KONUS experiments on Venera 11 and 12 have significantly enriched γ-ray burst phenomenology with spectral and temporal details for a large number of events (Mazets et al. 1981). Their low energy spectral features in the 30 to 70 keV range have been interpreted as due to cyclotron absorption and emission phenomena. We report high time-resolution (128 ms) spectral observations of γ-ray bursts with Solar Maximum Mission (SMM). We confirm the existence of deficiencies of low energy photons using extrapolated exponential-continuum fits from above 100 keV. Significant spectral variations, primarily at the lower energies, are also seen by SMM on time scales ≈ .25 s. Details of the SMM Hard X-Ray Burst Spectrometer (HXRBS) along with a previous analysis of one of the events discussed here have been given by Dennis et al. (1982). The event April 19, 1980 is reanalyzed and presented together with the events of April 21, 1980 and March 1, 1981.

Figure 1 shows the time-histories of these events for three energy bands covering the 25 to 500 keV range. April 19 and March 1 were relatively short events, ≈ 4 s and ≈ 2 s, respectively, compared to April 21, ≈ 20 s.

A Monte Carlo approach was utilized to simulate the HXRBS response to candidate spectral models, and thereby deconvolve the detector energy-loss spectra. Models representing thin thermal bremsstrahlung (TTB), thin thermal synchrotron (TTS) with and without absorption features, and power-law with exponential cutoff (PLE) were used to generate incident photon spectra. Best fits (least $\chi^2/\nu$) were obtained for the whole energy range by including absorption features at low energies (TTS and TTB). To study the evolution of the spectra, the events were subdivided into intervals corresponding to fine structures in the temporal profiles such as rising phase, decay phase, and valleys between pulses. This division is illustrated in Figure 1.

Figure 2 gives the photon energy spectra for the three events for the various intervals. The parameters for the best fits, adopting the TTS model, are indicated for various intervals of the events in Figure 2. For the two April events, the best fits are obtained by including absorption lines at low energy except for the valley intervals. The weak short event of March 1, 1981 exhibited a smooth continuum without

*Physics Department, University of Maryland, College Park, MD 20742
*From a Ph. D. dissertation performed at the University of Maryland.

ORIGINAL PAGE IS
OF POOR QUALITY



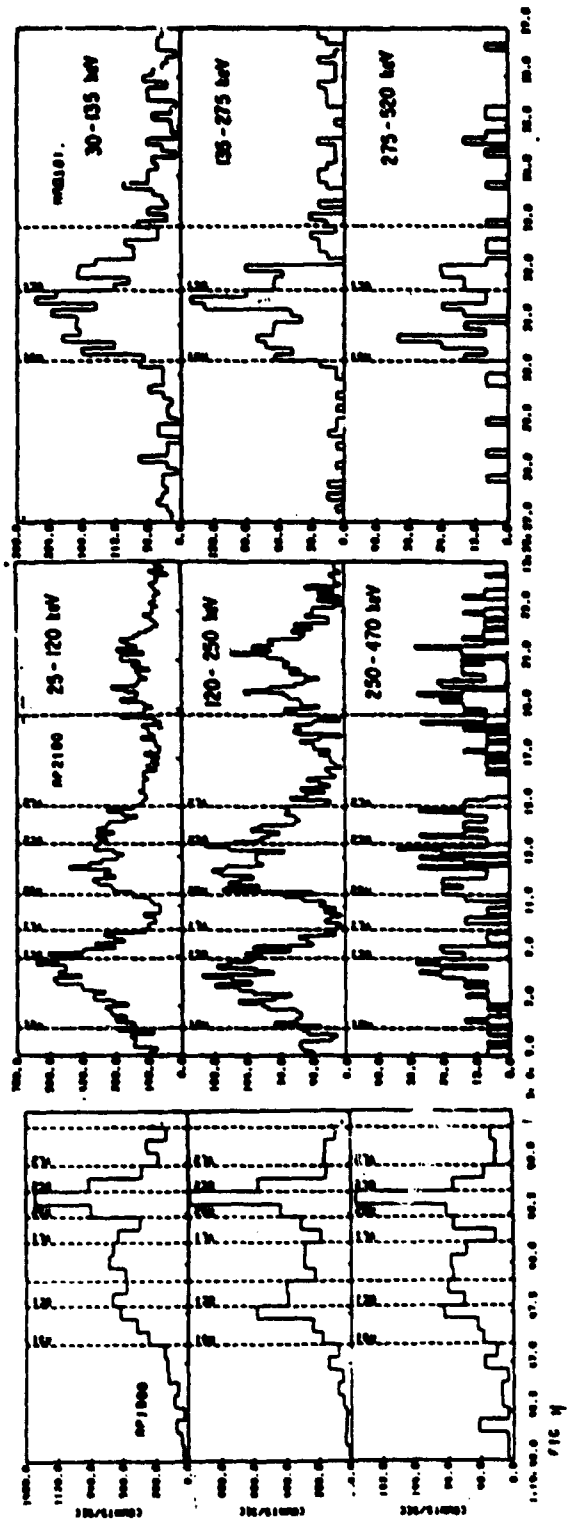


evidence of spectral features. The power-law portion of the PLE model provided acceptable fits to the low-energy channels without the inclusion of absorption features. The flattening in the spectra evidenced by the PLE model indicates, indeed, a depression or "shelf" at low energies.

Table 1 gives the values of the parameters for the TTS, TTB, and PLE models for intervals indicated in Figure 1. The parameters show significant variations during the course of the events. The values of kT in the TTB model have a wide dynamic range of 100 keV to 2 MeV. If one assumes a constant value for the magnetic field strength of ~ $10^{12}$ G, then the critical energies determined from the TTS model indicate a narrower range of temperatures, 180 keV to 570 keV. For both April events, Share et al. (1982) have fitted a power law to PHA data at higher energies up to 10 MeV.

From this analysis and recent results from the SIGNE experiment (Barat 1983), it is apparent that fast spectral evolution in γ-ray bursts may create the appearance of spectral features or camouflage actual features, and distort the continuum shape if spectra are integrated for intervals $\gtrsim$ 1 s.

ORIGINAL PAGE IS
OF POOR QUALITY



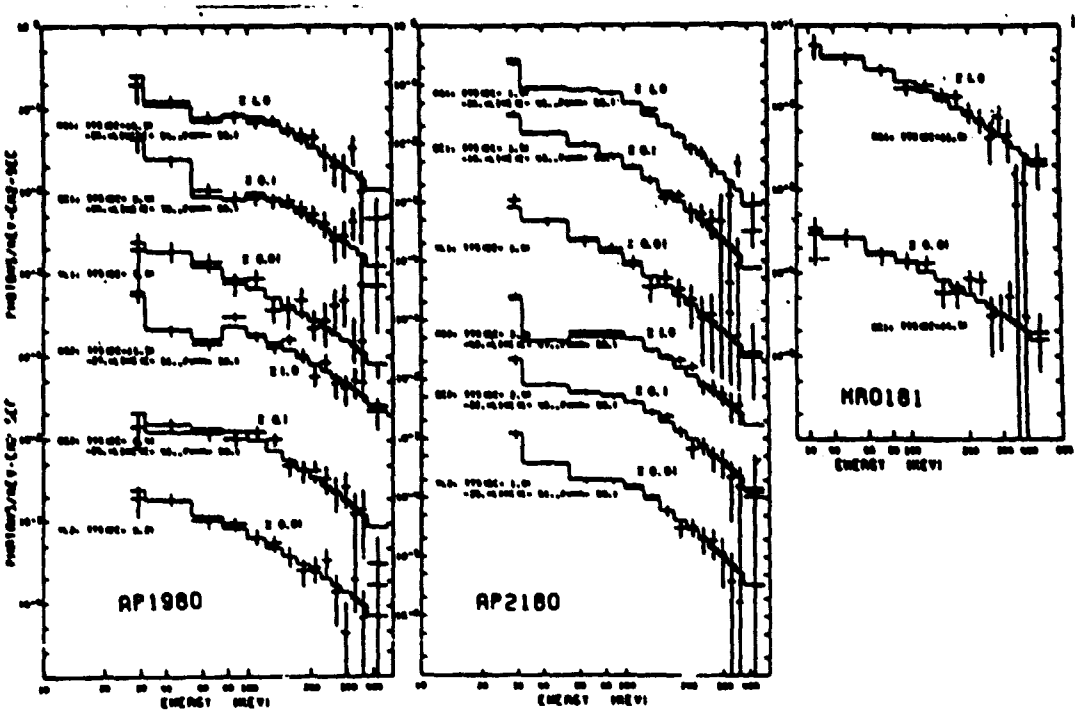


Figure 1

TABLE 1

* Thin Thermal Bremsstrahlung w/ w/o Absorption Line

| | $C_1$ | kT | $C_2$ | Energy | Width | $\chi^2/\nu$ |
|---|---|---|---|---|---|---|
| | | | AP1980 | | | |
| RS1 | 1.41±0.03 | 709±13 | 32.6±1.6 | 43.5±1.6 | 50.0±14.1 | 10.8/10 |
| DC1 | 2.19±0.13 | 604±33 | 36.2±5.0 | 55.±4.7 | 50.0±17.6 | 8.6/10 |
| VL1 | 0.63±0.57 | 1208±1177 | | | | 7.8/13 |
| RS2 | 3.19±0.05 | 781±11 | 36.0±1.0 | 48.5±1.0 | 33.0±2.2 | 12.0/10 |
| DC2 | 2.50±0.14 | 496±26 | 27.3±3.8 | 36.9±5.3 | 50.0±40.1 | 14.7/10 |
| VL2 | 0.79±0.38 | 947±347 | | | | 9.7/13 |
| | | | AP2180 | | | |
| RS1 | 9.06±0.23 | 103±2 | 37.6±1.3 | 4502±0.9 | 50.0±10.4 | 20.4/10 |
| DC1 | 4.74±0.19 | 128±4 | 10.4±2.8 | 41.8±9.3 | 33.0±26.9 | 8.2/10 |
| VL1 | 1.03±0.35 | 135±35 | | | | 5.0/10 |
| RS2 | 4.32±0.13 | 166±4 | 39.6±1.7 | 46.2±1.4 | 50.0±12.0 | 27.3/10 |
| DC2 | 4.54±0.48 | 148±10 | 36.6±4.8 | 46.5±2.8 | 50.0±29.0 | 6.2/10 |
| VL2 | 2.18±0.64 | 119±20 | 32.6±15.1 | 51.5±4.8 | 39.0±31.1 | 3.3/10 |
| | | | MR0181 | | | |
| RS | 0.10±0.02 | 1959±250 | | | | 14.5/13 |
| DC | 0.091±0.035 | 1514±586 | | | | 11.4/13 |

ORIGINAL PAGE IS
OF POOR QUALITY



# Thermal Synchrotron w/ w/o Absorption Line

AP1980

| | $C_1$ | $\varepsilon_c$ | $C_2$ | Energy | Width | $\chi^2/\nu$ |
|---|---|---|---|---|---|---|
| RS1 | 3.08±0.17 | 10.3±0.4 | 32.2±5.1 | 53.7±5.6 | 50.0±20.4 | 9.2/10 |
| DC1 | 5.35±0.31 | 8.4±0.3 | 34.1±5.1 | 69.8.±6.3 | 50.0±13.3 | 7.1/10 |
| VL1 | 2.55±1.60 | 9.9±4.7 | | | | 7.3/13 |
| RS2 | 6.23±0.26 | 11.5±0.4 | 26.8±3.4 | 51.4±4.3 | 33.0±10.1 | 13.3/10 |
| DC2 | 7.00±0.41 | 6.4±0.3 | 28.2±4.3 | 41.5±5.5 | 50.0±44.2 | 12.9/10 |
| VL2 | 2.77±1.10 | 9.2±3.0 | | | | 8.4/13 |

AP2180

| | | | | | | |
|---|---|---|---|---|---|---|
| RS1 | 52.2±10.9 | 1.4±0.1 | 35.8±4.6 | 44.5±1.9 | 50.0±26.9 | 22.9/10 |
| DC1 | 38.0±1.5 | 1.5±0.0 | 17.8±2.4 | 42.6±4.5 | 33.0±12.4 | 7.3/10 |
| VL1 | 4.88±0.37 | 1.9±0.1 | | | | 5.0/13 |
| RS2 | 18.6±0.6 | 2.3±0.0 | 41.9±1.7 | 47.3±1.3 | 50.0±9.9 | 31.2/10 |
| DC2 | 4.04±0.91 | 4.4±0.6 | | | | 12.7/13 |
| | 14.8±1.6 | 2.4±0.1 | 32.4±5.4 | 47.6±3.5 | 50.0±32.4 | 5.6/10 |
| VL2 | 2.49±0.69 | 3.3±0.6 | | | | 12.7/13 |
| | 13.0±4.4 | 1.6±0.2 | 34.7±12.6 | 50.7±3.8 | 40.9±26.7 | 3.4/10 |

MR0181

| | | | | | | |
|---|---|---|---|---|---|---|
| RS | 0.56±0.16 | 11.9±2.6 | | | | 11.1/13 |
| DC | 0.30±0.06 | 14.5±2.4 | | | | 10.2/13 |

# Power-law with Exponential Cutoff

AP1980

| | $C_1$ | $\alpha$ | $E_{cut}$ | $E_{char}$ | $\chi^2/\nu$ |
|---|---|---|---|---|---|
| RS1 | 1.04±0.05 | 0.57±0.01 | 196±18 | 146±37 | 4.5/11 |
| DC1 | 3.01±1.14 | 0.76±0.09 | 250±90 | 100±120 | 5.6/11 |
| VL1 | 2.40±0.58 | 0.78±0.05 | 338±163 | 19±130 | 7.7/11 |
| RS2 | 1.02±0.04 | 0.37±0.01 | 127±9 | 387±91 | 16.5/11 |
| DC2 | 0.89±0.93 | 0.46±0.24 | 132±37 | 171±77 | 9.7/11 |
| VL2 | 4.71±8.95 | 0.89±0.48 | 118±111 | 241±184 | 8.1/11 |

AP2180

| | | | | | |
|---|---|---|---|---|---|
| RS1 | 8.18±2.76 | 1.10±0.10 | 130±15 | 68±15 | 15.4/11 |
| DC1 | 15.2±4.8 | 1.22±0.09 | 73±28 | 102±20 | 8.8/11 |
| VL1 | 20.1±11.5 | 1.63±0.02 | 58±246 | 112±54 | 5.0/11 |
| RS2 | 3.46±1.50 | 0.95±0.10 | 193±29 | 63±26 | 15.2/11 |
| DC2 | 6.19±4.32 | 1.08±0.17 | 129±40 | 113±40 | 5.2/11 |
| VL2 | 5.46±4.48 | 1.27±0.20 | 124±49 | 99±44 | 8.0/13 |

Barat, C. 1983, preprint.
Dennis, B. R., et al. 1982, AIP Conference Proceedings No. 77, (New York: AIP), 153.
*Gould, R. J. 1980, Ap. J., 238, 1026.
Mazets, E. P., et al. 1981, Nature, 290, 378.
#Petrosian, V. 1981, Ap. J., 251, 727.
Share, G.H., et al. 1982 AIP Conference Proceedings No. 77,

ORIGINAL PAGE IS
OF POOR QUALITY



# DIFFUSE GALACTIC EMISSION OF HIGH ENERGY GAMMA RAYS

D.A. Kniffen, C.E. Fichtel, and R.C. Hartman
NASA/Goddard Space Flight Center
Greenbelt, Maryland 20771 U.S.A.

## 1. Introduction

Assuming cosmic rays pervade the Galaxy, they necessarily produce high energy γ-rays as they interact with the interstellar matter and photons. Substantial work has already been performed on the calculation of the source functions for these various γ radiations and the intensity to be expected in the vicinity of the solar system. (For a general review see Chapter 5 of Fichtel and Trombka, 1981.) However, several recent devlopments make a reexamination and extension of this work worthwhile. These include the recently published detailed results of high energy galactic γ-radiation obtained with the COS-B satellite (Mayer-Hasselwander et al., 1982) and the new COS-B background estimate (Strong, 1982), further evaluations of the 21 cm radiation in the galaxy and, hence, the atomic hydrogen density distribution, considerations related to the molecular hydrogen density normalization, and improved theoretical calculations on the nucleon-nucleon source function.

## 2. Gamma Ray Production and Intensity Calculations

The galactic matter distribution and content by species are discussed in earlier work (e.g., Kniffen, Fichtel, and Thompson, 1977), and only more recent consideration will be mentioned here. The density of neutral atomic hydrogen as revealed by the 21 cm emission remains somewhat uncertain in the inner galactic regions because of uncertainty in the absorption correction. Recent work (e.g. Dickey et al., 1982; Thaddeus, 1982) suggests that the absorption had previously been somewhat underestimated. Thus, in this work, the atomic hydrogen density distribution of Gordon and Burton (1976) as a function of radius from the galactic center was used, but modified so that the atomic hydrogen density in the innermost region was increased by a factor of 1.5, and the closer densities were increased less in accordance with the amount of intervening matter. Recent work by Lockman (1982) has, shown that the scale height is about 1 1/2 times larger then previously believed because a relatively faint component of HI had been overlooked. Hence, the scale height used in this work is 0.18 kpcs for a galactic radius, $R_{Gal}$, less than that of the sun (10.0 kpcs) and $[0.18 + 0.023 \times (R_{Gal} - 10.0)]$ kpcs for $R_{Gal} > 10.0$, with the incease beyond the solar circle being based on the work of Baker and Burton (1975). It is now believed that the scale height in the outer galaxy increases more rapidly than this (Kulkarni, Blitz, and Heiles, 1982), but the surface density is still believed to be similar to earlier estimates. The density distribution of molecular hydrogen is measured less directly than that of atomic hydrogen, and hence the absolute value of the density is less certain. In this work the galactic distribution of Gordon and Burton (1976) was used, but density normalization was treated as an adjustible parameter.

Although the translation of the 21 cm observations into a galactic spatial distribution is difficult, on a broad scale the density profile

ORIGINAL PAGE IS
OF POOR QUALITY



is reasonably well known, even though details of arm structure are not always agreed on by all workers in the field. Until recently, it had not been clear whether molecular clouds were associated with spiral structure. However, now on the basis of a high sample survey and observations in both the first and second quadrants of the galactic plane, Cohen et al. (1980) have reported the existence of the molecular counterparts of the five classical 21 cm spiral arms segments in these quadrants. The specific spiral pattern that will be used here is that of Georgelin and Georgelin (1976). A five hundred parsec width is adopted for the arms. The excess of material in the arms is taken to be the smaller of 25% of the total local matter or twice the local average density of matter not in the arms, based on recent considerations (Lockman, 1982, and Kulkarni, Blitz, and Heiles, 1982).

For the photon distributions, Kniffen and Fichtel (1981), using results of Boissé et al. (1981) on the infrared volume emissivity and a model of Bahcall and Soneira (1980) for the starlight distribution, obtained photon densities and, hence, source function for the Compton emission as a function of position in the galaxy.

With regard to the cosmic ray distribution in the galaxy, it will be assumed that the nucleonic cosmic ray composition and energy spectrum remain unchanged throughout the galaxy and that the electron spectrum changes only in a second order manner as the density changes. (See particularly Kniffen and Fichtel, 1981, and Fichtel et al., 1976) For the reasons described in the above works, the cosmic ray density in the plane will be assumed to be proportional to the matter density on the scale of arms and, perpendicular to the plane, to have a gaussian distribution with a scale height of 0.6 kpc. This latter number is based on the radio continuum measurements of Cane (1977) and the assumption that the galactic magnetic field energy density and the cosmic ray energy density have the same scale height.

The production functions and intensity calculations are essentially the same as earlier work with the exception of the source function for cosmic ray nucleon matter interactions. Badhwar and Stephens (1977), Stephens and Badhwar (1981), and Morris (1982) have used the substantial recent high energy physics experimental work to estimate the γ-ray production energy spectrum for cosmic rays interacting with interstellar matter. The spectral shapes calculated by Badhwar and Stephens (1977) and Morris (1982) are similar. Both are, however, significantly different from the earlier pioneering work based more heavily on theoretical models when the more extensive experimental data were not available. The Morris (1982) work was used here.

## 3. Results

The γ-ray intensity predicted by this work is compared to the COS-B longitude distributions in Figure 1. It should be mentioned that COS-B scientific group has recently reanalyzed the instrumental γ-ray background (Strong, 1982). Whereas the background intensities for the (150-300) MeV and the (300-5000) MeV energy intervals are essentially unchanged from the paper of Mayer-Hasselwander et al. (1982), the (70-150) MeV background intensity is now estimated to be $5.6 \times 10^{-5}$ photons $cm^{-2}s^{-2}$ $ster^{-1}$, a factor of ~1.75 higher. This change has been incorporated in Figure 1 by introducting a new "zero base". The revision

ORIGINAL PAGE IS
OF POOR QUALITY



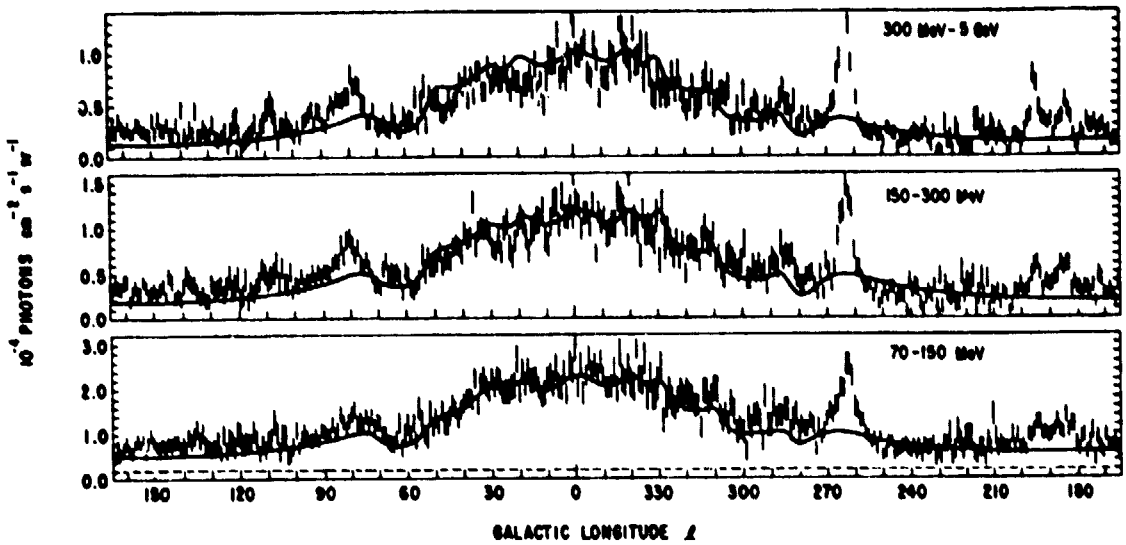


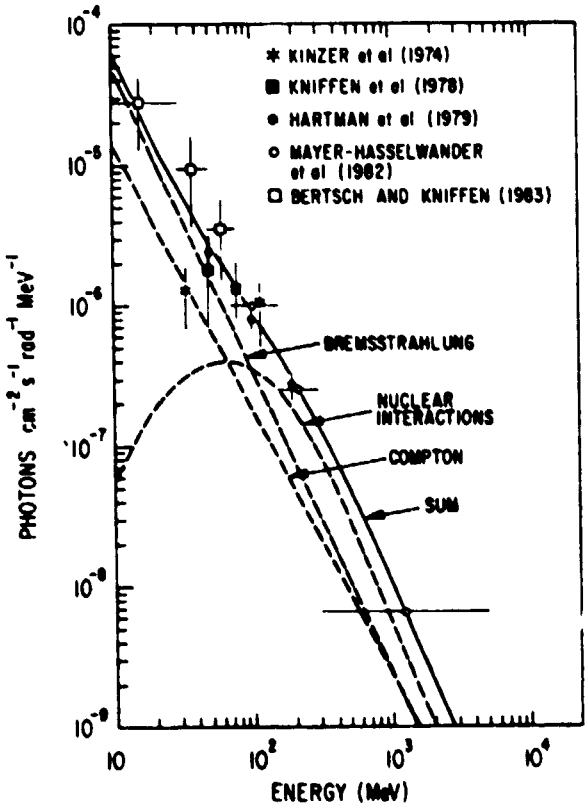


Figure 1: Gamma ray intensity as a function of longitude averaged over the latitude range $-10° < b < 10°$ from 70 MeV - 150 MeV, 150 MeV - 300 MeV, and 300 MeV - 5000 MeV from the COS-B data (Mayer-Hasselwander et al., 1982) compared to the model discussed here shown by the solid line. The dashed line in the 70-150 MeV graph represents the new "0.0" line based on the revised background intensity for the COS-B data in this energy interval discussed in the text.

Figure 2: Energy spectrum of the galactic $\gamma$ radiation for a region near the galactic center. The calculated spectra are based on the work of Kniffen and Fichtel (1981) modified to include the recent nucleon-nucleon calculations of Morris (1982). The COS-B data are those of Mayer-Hasselwander et al. (1982), and the SAS-2 data are those of Hartman et al. (1979).

means that not only are the intensities for the center and the sources (195,5), PSR 0531+21, PSR 0833-45 measured with the SAS-2 and COS-B instruments in good agreement with each other, but also the general galactic diffuse intensity. It was noted earlier in this article that molecular hydrogen density normalization was left as an adjustable para-

ORIGINAL PAGE IS
OF POOR QUALITY



meter. There did need to be an adjustment for the inner ring by a factor of about 0.7, but no adjustment was required beyond this ring. Regarding Figure 1 and the energy spectrum shown in Figure 2, considering the uncertainty in the point source contribution and the mass distribution, the agreement between the data and the predicted curves seems reasonably good especially when the known discrete sources are taken into account.

The latitude distributions resulting from the model have been calculated taking into account the COS-B instrument response. The fit to the galactic center observations is remarkably good at all energies. This gives confidence that not only is the total observed emission well predicted by the model, but also that the radial distribution of the emission calculated from the model must also be approximately correct. The anticenter result is reasonable considering the uncertainty of the γ-ray measurements and the gas distribution in that general direction. At $\ell$=70 to 90, the overall intensity prediction is about right, but there is some indication in all energy intervals that the average emission may be slightly more distant than the model prediction.

It should also be mentioned that in the concept being presented here the arms on the far side of the galaxy make an important contribution for small ($|b| \lesssim 0.4°$) galactic latitudes. With future high resolution γ-ray measurements, these back side arms should appear as a narrow ridge superimposed on the broader ridge of the near side arms. It may be possible to identify very large far side molecular clouds if the majority of the molecular hydrogen is in large clouds.

**REFERENCES**

Badhwar, G.D., and Stephens, S.A.:1977, 15'th Int. Cos. Ray Conf., 1, 198.
Bahcall, J.N., and Soneira, R.M.:1980, Ap. J., 238, L17.
Baker, P.L., and Burton, W.B.:1975, Ap. J., 198, 281.
Bignami, G.F., et al.:1975, Ap. J., 199, 54.
Boissé, P., et al.:1981, Astr. Ap., 94, 265.
Cane, H.V.:1977, Ph. D. Thesis, University of Tasmania, Hobart.
Cohen, R.S., et al.:1980, Ap. J. (Letters), 239, L53.
Dickey, J.M., et al.:1982, Low Latitude Absorption Spectra, NRAO Doc.
Fichtel, C.E., et al.:1976, Ap. J., 208, 211.
Fichtel, C.E., and Trombka, J.I.:1981, Gamma Ray Astrophysics, New Insight into the Universe, NASA SP-453.
Georgelin, Y.M., and Georgelin, V.P.:1976, Astron. Astrophys., 49, 57.
Gordon, M.A., and Burton, W.B.:1976, Ap. J., 208, 346.
Hartman, R.C., et al.:1979, Ap. J., 230, 597.
Kniffen, D.A., and Fichtel, C.E.:1981, Ap. J., 250, 389.
Kniffen, D.A., Fichtel, C.E., and Thompson, D.J.:1977, Ap. J., 215, 765.
Kulkarni, S.R., Blitz, L., and Heiles, C.:1982, Ap. J., 259, L63.
Lockman, F.J.:1982, preprinted, "The HI Halo in the Inner Galaxy."
Mayer-Hasselwander, H.A., et al.:1982, Astron. Astrophys., 105, 164.
Morris, D.J.:1982, Ph. D. Thesis, University of Maryland.
Stephens, S.A., and Badhwar, G.D.:1981, Astrophys. & Space Science, 213.
Strong, A.W.:1982, private communication on behalf of the COS-B group.
Strong, A.W., et al.:1982, submitted to Astron. and Astrophys.
Thaddeus, P.:1982, private communication.

ORIGINAL PAGE IS
OF POOR QUALITY

# ELECTRON PROPAGATION IN THE LEAKY BOX MODEL WITH A TRUNCATED PATHLENGTH DISTRIBUTION

B. G. Mauger* and J. F. Ormes
NASA/Goddard Space Flight Center, Greenbelt, MD 20771, U.S.A.

## 1. INTRODUCTION

Early studies (Ormes and Freier, 1978; Protheroe, Ormes, and Comstock, 1981) of the chemical composition of cosmic ray nuclei with $3 < Z < 28$ suggested that observed primary cosmic ray spectra have been steepened by a factor of $E^{-.4\pm.1}$ from their source spectra, suggesting source spectra that vary as $E^{-2.5\pm.1}$. Electrons, at high energies will be steepened by energy losses by a factor of $E^{-1}$ from their source spectrum. Electron data above 20 GeV exhibits a spectrum as steep as $E^{3.3}$ which is consistent with an $E^{-2.3}$ source spectrum.

Recent studies using HEAO-3 data (Ormes and Protheroe, 1983) and balloon data (Simon and Mathis, 1983) now suggest an escape steepening of $E^{-.7\pm.1}$. These studies imply a source spectrum of $E^{-2.0\pm.1}$, which in turn suggests an energy steepened electron spectrum of $E^{-3.0\pm.1}$, which is inconsistent with the electron data. In this paper, the authors suggest that a truncated pathlength distribution due to a lack of nearby sources could be responsible for the additional steepening of the electron spectrum.

## II. Electrons in the Leaky Box Model

In the leaky box model it is assumed that cosmic rays are injected into the galaxy with a power law energy spectrum, $N(E) = N_o E^{-\Gamma_o}$, and escape in an energy dependent manner with an average escape lifetime, $\tau_{EX} = \tau_o E^{-\delta}$. It is also assumed that these sources are homogeneously distributed and that cosmic rays diffuse from these sources throughout the galaxy. This suggests an exponential age distribution:

$$P(t) = \frac{dt}{\tau_{EX}(E)} \exp(-t/\tau_{EX}(E)).$$

Due to cosmic ray electrons' energy losing interactions with the interstellar electromagnetic fields, electrons have a second characteristic lifetime. This second lifetime is an energy loss lifetime, $\tau_{EN} = 1/bE$, where b is a constant depending only on the galactic electromagnetic fields.

Using this model, Silverberg and Ramaty (1973) and Ramaty (1974) have modeled the electron propagation. These authors demonstrate that if $\delta < 1$, at low energy the electron lifetime will be dominated by

* NAS/NRC Research Associate

escape ($\tau_{EX} \ll \tau_{EN}$), and at high energy the electron lifetime will be dominated by energy loss ($\tau_{EN} \ll \tau_{EX}$). The equilibrium electron spectrum will be the injection spectrum steepened by escape at low energies ($N(E) \propto E^{-(\Gamma_o + \delta)}$) and will be the injection spectrum steepened by energy loss at high energies ($N(E) \propto E^{-(\Gamma_o + 1)}$).

## 3. A Truncated Pathlength Distribution

In reality, the distribution of cosmic ray sources is not uniform. The distance to the nearest cosmic ray source will determine some minimum lifetime for any observed cosmic rays. In this work, the authors have used a truncated age distribution of the form:

$$P(\tau)d\tau = \frac{d\tau}{(\tau_L - \tau_S)} (\exp(-\tau/\tau_L) - \exp(-\tau/\tau_S))$$

where $\tau_{EX} = \tau_L + \tau_S$. $\tau_S(E)$ is the time it takes for a cosmic ray of energy E to diffuse to the solar system from the nearest source(s), and $\tau_L$ is the average storage lifetime in the galaxy. If the energy dependence of cosmic ray propagation is assumed to be uniform throughout the galaxy, then $\tau_S$ and $\tau_L$ are also propoirtional to $E^{-\delta}$. This age distribution is identical to the age distribution of Cowsik and Wilson's (1975) two-zone distribution, except that $\tau_S$ now characterizes the local storage volume rather than that of the sources.

Suppose $\tau_S = f\tau_{EX}$, where f is some constant fraction then:

$$\tau_S = f\tau_o E^{-\delta} \text{ and } \tau_L = (1-f)\tau_o E^{-\delta}.$$

Considering only synchrotron and Compton energy losses, the equilibrium electron flux obeys the equation (Silverberg and Ramaty, 1973):

$$\frac{d}{dE}(bE^2 N(E)) + \frac{N(E)}{\tau_{EX}(E)} = Q(E)$$

with the source spectrum, $Q(E) \propto E^{-\Gamma_o}$, the electron flux can be calculated for this truncated pathlength distribution to be:

$$N(E) = N_o E^{-(\Gamma_o+1)} \int_1^\infty d\epsilon\, \epsilon^{-\Gamma_o} [\exp(-y/(1-f)) - \exp(-y/f)]$$

where

$$y = \frac{\tau_{EN}}{\tau_{EX}} \frac{(1-\epsilon^{\delta-1})}{1-\delta} \text{ and } \epsilon = (1-bE\theta)^{-1}$$

The variable of integration, $\epsilon$, is a function dependent on $\theta$, the amount of time since the electron left its source. Since $\tau_{EN} \propto E^{-1}$ and $\tau_{EX} \propto$

$E^{-\delta}$, $y = E^{-(1-\delta)}$ and y approaches zero as E increases, at some very large E it is possible to use the linear approximations:

$$\exp(-y/(1-f)) = 1 - y/(1-f) \text{ and } \exp(-y/f) = (1-y/f)$$

Using these substitutions, the electron flux can be written as:

$$N(E) = E^{-(\Gamma_o + 1)} \frac{\tau_{EN}}{\tau_{EX}} \int_1^\infty dt\, t^{\Gamma_o} \left(\frac{1}{t} - \frac{1}{1-t}\right) \frac{(1-t^{\delta-1})}{(1-\delta)}$$

The integral is now independent of E and is a constant, and at very high energy we see:

$$N(E) \propto E^{-(\Gamma_o + 1)} \tau_{EN}/\tau_{EX} \propto E^{-(\Gamma_o + 2 - \delta)}.$$

The injection spectrum has been steepened by a factor of $(2 - \delta)$.

## 4. Discussion

The above shows that the lack of nearby sources can steepen the injection electron spectrum by more than one power of E. The electron spectrum can be broken into three regions. The first is the low-energy region where electron storage is dominated by escape, $\tau_{EX} < \tau_{EN}$. The slope of the electron spectrum, like other primary species, is the slope of the injection spectrum steepened $\delta$ by escape. The second region is the medium energy region where $\tau_S < \tau_{EN} < \tau_{EX}$. In this region, the electron energy loss lifetime is sufficiently short to dominate propagation, but not so short as to prevent electrons from propagating throughout the storage region. In this second region, the slope of the spectrum is equal to that of the injection spectrum steepened by one power of energy. The third region is very high energy where $\tau_{EN} < \tau_S$. This is the energy region in which the energy loss lifetime is shorter than the time it takes for cosmic rays to diffuse to Earth from the nearest source. This produces a further steepening in the electron spectra.

The salient point of this calculation is that the asymptotic slope of the electron spectrum can be steeper than that of the injection spectrum by more than one power of energy. Figure 2 shows the electron spectra above 1 GeV as measured by Nishimura et al. (1980) and Prince (1979). The steepening of the electron spectra appears to occur in the region of 20-50 GeV. For this steepening to occur due to a truncated age distribution, at 50 GeV:

$$\tau_S = f\tau_{EX} > \tau_{EN} = (bE)^{-1}$$

The energy loss coefficient, b, has the value

$$b = (3.79 \times 10^{-18}\, E_T^2 + 1.02 \times 10^{-16}\, \rho_{PH})(\text{GeV-s})^{-1}$$

ORIGINAL PAGE IS
OF POOR QUALITY



where $H_T$ is the average transverse magnetic field in microgauss and $\rho_{PH}$ is the photon energy density in $eV/cm^3$. Using the values of 5μG for $H_T$ and .7 $eV/cm^3$ for $\rho_{PH}$, $b = 1.66 \times 10^{-16}$ $GeV^{-1}$ $s^{-1}$. For this value of b, at 50 GeV one gets an energy loss lifetime of 3.8 million years. Using a value of .2 for f, $\tau_{EX}$ must be on the order of 20 million years at 50 GeV. If one assumes the same storage time rigidity dependence as derived by Ormes and Protheroe (1983) for the escape length, then this lifetime could be a factor of two longer at 1 GV/c. This can be compared with the 10-20 x $10^6$ year lifetime measurements at 1 GV/c based on the $^{10}Be$ isotope (Wiedenbeck and Greiner, 1980). Assuming these lifetimes should be the same implies that the root mean square magnetic field must be in the range of 8-10μG.

Although the truncated age distribution provides an attractive method for steepening the electron spectrum, it requires that cosmic rays are either stored in the galaxy longer than currently believed, or the magnetic field traversed by the cosmic rays must be higher than the 5μG used in the above calculation.

## References

Cowsik, R. and Wilson, L. W., 1975, Proc. 14th Int. Cosmic Ray Conf., 2, 659.
Nishimura, J. et al., 1980, Ap. J. 218, 394.
Ormes, J. F. and Freier, P. S., 1978, Ap. J., 222, 471.
Ormes, J. F. and Protheroe, R. J., 1983, Ap. J., in press.
Prince, T. A., 1979, Ap. J. 227, 676.
Protheroe, R.J., Ormes, J.F., and Comstock, G.M., 1981, Ap. J., 247, 362.
Ramaty, R., 1974 in High Energy Particles and Quanta in Astrophysics, ed. C. Fichtel and F. B. McDonald (Cambridge: MIT Press).
Silverberg, R. F. and Ramaty, R., 1973, Nature 243, 134.
Simon, M. and Mathis, K. D., submitted to Astronomy and Astrophysics.
Wiedenbeck, M. E. and Greiner, D. E., 1980, Ap. J. 239, L139.

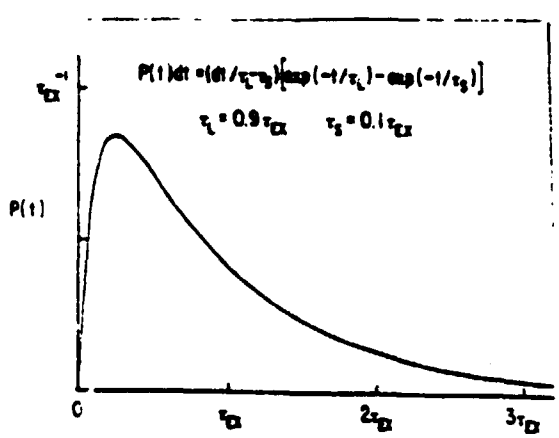


Figure 1. A truncated age distribution based on the two-zone model.

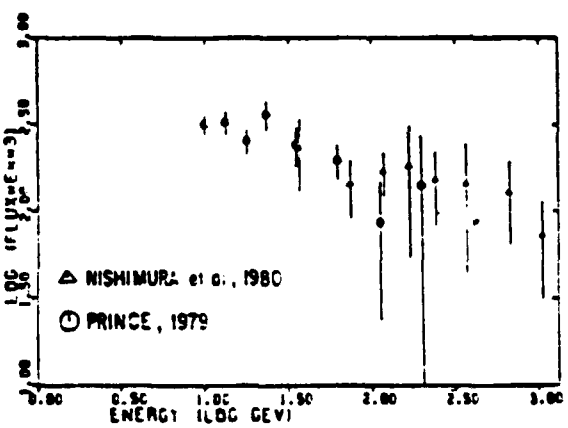


Figure 2. Electron data above 5 GeV.

ORIGINAL PAGE IS
OF POOR QUALITY



# LOCAL SUPERBUBBLE MODEL OF COSMIC RAY PROPAGATION

R. E. Streitmatter, V. K. Balasubrahmanyan, and J. F. Ormes
NASA/Goddard Space Flight Center, Greenbelt, MD 20771, U.S.A.

R. J. Protheroe
Dept. of Physics, University of Adelaide, South Australia 5001

## I. INTRODUCTION

Considerations of the lifetime, L/M ratio, low anisotropy, and high energy electron spectrum suggest that observed cosmic rays propagate in a local space of dimensions less than 1 kpc. Kafatos et al. (1981) have suggested that the solar system may be inside a superbubble (Heiles, 1979) which confines local cosmic rays. Bruhweiler et al. (1980) and Tomisaka et al. (1981) have shown that the shell-like structure of superbubbles may result from the sequential explosions of supernovae in evolving OB associations. In this paper we explore the consequences for cosmic ray phenomena of the solar system being inside a superbubble which we suggest should be identified with the expanding ring of HI (Feature A), which was first observed by Lindblad (1967). Figure 1 shows the ring relative to the solar system in the plane of the galaxy. Figure 2 is a model of the local galactic plane magnetic field, which has been largely excluded from the superbubble by being swept up as matter is "snow-plowed" outward by the superbubble expansion.

## II. LOW ENERGY COMPOSITION AND ENERGY SPECTRA

The radius of the superbubble at age t is proportional to t**(0.5). This expansion with time causes the contained relativistic cosmic rays to lose energy as dE/dt = (-1/2)(E/t). We shall adopt this energy loss law also for non-relativistic particles. This may result in some underestimation of matter traversal and superbubble age from low energy data. We assume that the injection rate of nuclei of type i of energy E (per nucleon), $Q_i(E)$, is constant. The region inside the superbubble is of low density. Cosmic ray particles traverse the inside region relatively freely, interact with the dense walls of the superbubble, and accumulate grammage in repeated wall encounters throughout their lifetime. On average, over repeated wall encounters, the rate of matter traversal by cosmic rays (in g $cm^{-2}$ per second) is taken as independent of t and parameterized as X(E)/T where T is the present age of the superbubble.

The number and energy spectrum of nuclei of type i contained within the superbubble throughout its history is given by:

$$\frac{\partial N_i(E,t)}{\partial t} = Q_i(E) + \frac{1}{T} \sum_{j>i} N_j(E,t) \frac{X(E)}{X_{ji}} - N_i(E,t) \left\{ \frac{1}{T} \frac{X(E)}{X_i} + \frac{1}{t_D^i(E)} \right\} + \frac{\partial}{\partial E} \left\{ \frac{1}{2} \frac{E}{t} N_i(E,t) \right\}, \quad (1)$$

where: $X_i$ is the interaction length (g $cm^{-2}$) of species i; $X_{ji}$ is the transformation length for j → i; $t_D^i(E)$ is the mean radioactive decay time of species i.

Because of the superbubble's expansion, particles observed now with energy E had energy E' = E x (τ**(-1/2)) when produced at epoch τ ≡ t/T. Solving equation (1) for the present spectrum, we obtain:

$$N_i(E, \tau = 1)dE = \int_0^1 P_i(E',\tau)dE' \; \theta(E,\tau) \; \phi(E,\tau)d\tau, \quad (2)$$

where $P_i(E', \tau)dE' = \{Q_i(E')T + \sum_{j>i} N_j(E',\tau) \frac{X(E')}{X_{ji}}\} \tau^{-1/2} dE'$. (3)

In equation (2), $\theta(E,\tau)$ and $\phi(E,\tau)$ are the probabilities of a nucleus of present energy E having survived nuclear interaction or radioactive decay respectively from production at an earlier epoch, $\tau$, with energy E x ($\tau$**(-1/2)).

For a primary species injected uniformly throughout the history of the superbubble with a power law energy spectrum with exponent $-\gamma$,

$$P_i(E',\tau)dE' = \tau^{(\gamma-1)/2} Q_i(E)TdE. \quad (4)$$

The quantity analagous to the age distribution of primaries in conventional models is $\tau$**((γ-1)/2) and we will refer to it as such. For $X(E) = E^{-\nu}$, the age distribution of secondary species is approximately proportional to $\tau$**(1 + (γ + ν - 1)/2). These age distributions have been plotted in Figure 3 for γ = 2.7 where they are compared to age distributions in the leaky-box model (exponentials) for various mean escape times, $t_{esc}$.

Present spectra are similar to production spectra, e.g., primaries at high energy ($X \ll X_i$) have $N_i(E) = 0.54\ Q_i(E)T$ for γ = 2.7 (the 0.54 factor is due to expansion). Although the age distributions of primary and secondary nuclei are intrinsically different, secondary and primary energy spectra differ mainly because of the assumed energy dependence of X(E). Predicted secondary to primary ratios using $X = 7$ g cm$^{-2}$ for ($E \lesssim 2$ GeV/nuc) and X = 7 (E/2 GeV/nuc)**(-0.33) g cm$^{-2}$ for (E > 2 GeV/nuc) give a good fit to the observations (e.g., data surveyed by Protheroe, et al., 1981). Using the observed surviving fraction of $^{10}$Be (Garcia-Munoz et al., 1977) and equations (2)-(3), we obtain T = (2.9, +1.3, -0.7) x 10**7 years, consistent with the astrophysical estimate of the age of Feature A (Olano, 1982). This is just what we expect based on Figure 3 where we see that the age distribution of young secondaries is very similar to that in the leaky-box model provided T is about 2.3 times the mean escape time, $t_{esc}$, that would be obtained if the leaky box model had been used to interpret the data.

## III. HIGH ENERGY COSMIC RAYS

The local superbubble model offers a natural explanation for features in the high energy cosmic ray anisotropy and spectrum which occur around 10**15 eV (see the review of Linsley, 1981). We interpret these as due to failure of the superbubble wall to contain cosmic rays of high energy. At energies well below 10**15 eV, the wall is assumed to trap completely incident particles. However, at high energies the wall becomes more permeable to cosmic rays and there is an energy dependent probability G(E) that a particle striking the wall will escape. This is related to the high energy anisotropy: $\delta(E) = G(E)\ \Delta\rho(E)/\rho(E)$ where ρ is the cosmic ray density and Δρ is the difference in density between cosmic rays inside and outside the superbubble.

At high energies, where we can neglect nuclear interactions, the number of cosmic ray nuclei of type i within the superbubble is given by:

$$\frac{\partial N_i(E,t)}{\partial t} = Q_i(E) + \frac{\partial}{\partial E}\{\frac{1}{2}\frac{E}{t} N_i(E,t)\} + \{\rho_i(E)V(t) - N_i(E,t)\}/t_L^i(E,t) \quad (5)$$

where E is now taken to be the total energy per nucleus, V is the superbubble's volume, $\rho_i$ is the exterior cosmic ray density of species i, and $t_L^i$ is the mean leakage time (in or out) of species i. We shall assume a rigidity dependence for the leakage time of species i (atomic number z), $t_L^i(E) = \langle t\rangle(E/zE_o)^{-\sigma}$ where $\langle t\rangle$ is the mean cosmic ray age (~ 0.4 T) and $E_o$ is the energy at which the present leakage time of protons is equal to $\langle t\rangle$. For the exponent of the escape law, we shall use

$\alpha = 0.6$, the power law exponent of the observed anisotropy above 10**14, since the escape probability is approximately proportional to $\delta$. (We can neglect the energy dependence of $\Delta\rho/\rho$ unless the exterior spectrum is steeper than the interior spectrum). Equation (5) may be solved in two extreme cases for the energy spectrum at the present time ($t = T$) to yield:

$$N_i(E) = \begin{cases} Q_i(E)T/[1 + \frac{1}{2}(\gamma-1)] & \text{(Expansion dominates)} \\ \{\rho_i(E)\, V + Q_i(E)\, t_L^i(E)\}\{1-\exp[-T/t_L^i(E)]\} & \text{(Leakage dominates)} \end{cases} \quad (6)$$

For the purpose of illustration, we consider cosmic rays to be composed solely of protons and Fe-nuclei. In Figure 3 we show spectra and relative abundances calculated using an approximate solution to equation (5), which agrees asymptotically with equation (6), for three representative sets of parameters. In case I, the parameters represent minimum assumptions required to obtain agreement with the observed total energy spectrum: the spectra produced inside and outside the superbubble are normalized to data at 10**10 eV and 3 x 10**18 eV respectively and taken to have the same differential spectral index $\gamma = 2.7$. $E_o$ has been chosen as 2 x 10**15 eV and, at a given total energy, a production ratio p:Fe of 3:1 has been used. Figure 3(b) shows components of the differential spectrum from interior and exterior sources. Case II is a modification of Case I in which a spectral index of $\gamma = 3.05$ has been used for spectra exterior to the superbubble and $\alpha$ has been set equal to 0.8. This causes the spectra from the exterior to dominate at all energies above ~ 10**15 eV and produces a bump-like feature at ~ 10**15eV. Case III is a modification of Case I in which Fe is injected with a flatter spectrum ($\gamma = 2.6$) and $E_o$ is lowered to 3 x 10**14 eV. As seen in Figure 3(c), this results in an enhanced Fe composition consistent with the Maryland result (Goodman et al., 1979)--(hatched area) and the Durham group (Chantler, et al., 1983)--(vertical bands).

In the energy range from 3 x 10**14 eV to 10**17 eV, the direction of the measured anisotropy (See Linsley, 1981; Watson, 1982) is RA ~ 12-18 h indicating a net local flow from the nearby wall (see Figure 1). Although this might imply a higher cosmic ray density at these energies outside the superbubble, this is unlikely since the leakage time constants above 10**15 eV become much less than the cosmic ray age; a significant net inflow cannot then be sustained. Thus, the direction of observed anisotropies from 10**15 eV to 10**17 eV is probably a transient of duration much less than <t>. Possibilities include: a) Cosmic rays from exterior sources in the Sco-Cen active region may be "seen" through the partly transparent superbubble wall; b) A mini-superbubble (Davelaar, et al., 1980) may surround the Sco-Cen region (Loop I, the North Polar Spur, may be the intersection of the two superbubbles) and contain a higher cosmic ray density which is now leaking into our superbubble; c) We are just seeing an anisotropy from the nearest (wall) source. Just above 10**17 eV, the abrupt reversal in the observed anisotropy direction indicates a return to net outward flow of cosmic rays toward the local wall. This persists until about 5 x 10**18 eV, the apparent energy at which the anisotropy ceases being dominated by the local wall.

References

Bruhweiler, F. C., et al., 1980, Ap. J., 238, L27.
Chantler, M. P., et al., 1983, J. Phys. G. 9, L27.
Davelaar, J. A., et al., 1980, Astron. and Astrophy., 92, 231.
Garcia-Munoz, M., et al., 1977, Ap. J., 217, 859.
Goodman, J. A. et al., 1979, Phys. Rev. Lett., 42, 854.
Heiles, C., 1979, Ap. J., 229, 533.
Kafatos, H., et al., Ap. J., 1981., 2, 222.
Lindblad, P. O., 1967, Bull. Astr. Inst. Netherlands, 19, 34.

ORIGINAL PAGE IS
OF POOR QUALITY



Linsley, J., 1981, IAU Symp. 94, 53.
Olano, C. A., 1982, Astron. Astroph., 112., 195.
Protheroe, R. J., et al., 1981, Ap. J., 247, 362.
Tomisaka, K., et al., 1981, Astr. and Sp. Sci., 78, 273.
Watson, A. A., 1982, Proc. 1st Moriond Astrophysics, 49.

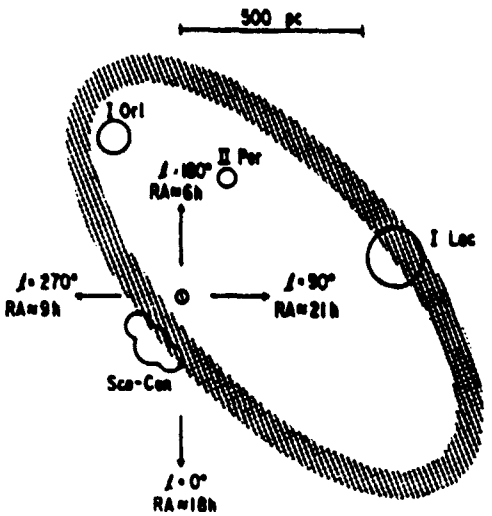


Figure 1

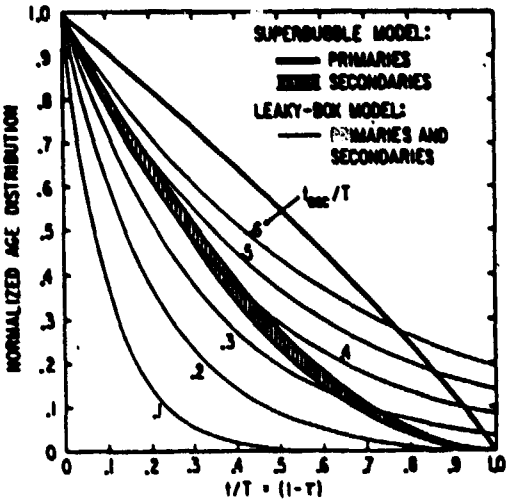


Figure 3

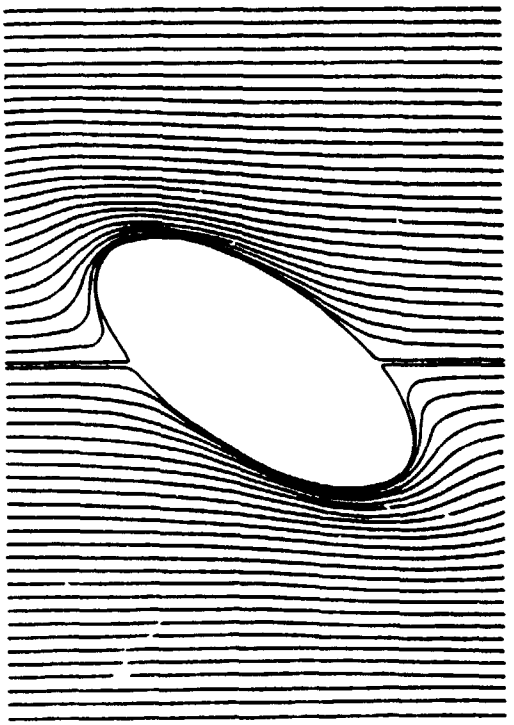

Figure 2

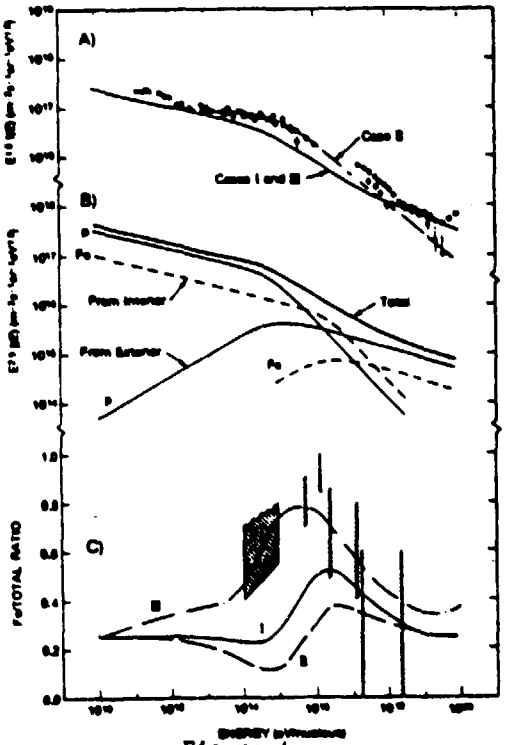


Figure 4

ORIGINAL PAGE IS
OF POOR QUALITY



# ON THE LOCALIZED NATURE OF THE GALACTIC COSMIC RAYS

J. F. ORMES
NASA/Goddard Space Flight Center
Greenbelt, MD 20771 USA

## 1. Introduction

The recent observations of charge composition data from the HEAO-3 satellite (Engelmann et al., 1981), have been interpreted (Ormes and Protheroe, 1983) to suggest that the escape of cosmic rays from the galaxy at rigidities above 10 GV/c falls more rapidly then previously thought $\lambda_e \propto R^{-\delta}$, ($\delta = 0.7 \pm 0.1$ compared to earlier values in the range $0.3 \lesssim \delta \lesssim 0.5$). If one associates this steep rigidity dependence with the diffusive escape of particles from the galaxy, and further connects it with the energy dependence of the anisotropy above $10^5$GV/c, one is led to speculate that the diffusion coefficient of 10 GV/c cosmic rays may be as low as $10^{26-27}$cm$^2$/sec. In this paper we explore the consequences of such a low value of the diffusion coefficient and of various values of $\delta$. We then address consequences for the propagation of cosmic rays, in particular their localization near their point of origin sufficient to explain the roleover the escape of low energies.

## 2. The Diffusion Coefficient

Consider a model in which the diffusion coefficient is isotropic throughout all space, and the sources are confined to the galactic disk (e.g., where SN are occurring). It can be shown that the spectra integrating over the finite disk and for all time give power law spectra steepened from the source spectra by the power $\delta$ with which the diffusion coefficient varies as the rigidity (Streitmatter and Balasubrahmanyan, 1983).

The observed cosmic ray proton spectrum is presumed to be due to the injection spectrum, perhaps from shock acceleration, steepended by the energy dependence of the diffusive escape of particles from the galaxy. Since the proton spectrum has the form of a power law without change of slope from 10 GV/c up to $10^5$GV/c (Gregory et al., 1981), we assume that the energy dependence of the escape holds up to at least this energy and that it is represented by a diffusion coefficient which is also a power law in rigidity. We take for discussion purposes a diffusion coefficient as shown in Figure 1, the exponents shown being $\delta = 0.5$ and $\delta = 0.7$ as determined by the energy dependence of the escape. The former value comes from the preliminary analysis of balloon (e.g., Garcia-Munoz et al., 1981) and HEAO-3 data (Perron et al., 1981) whereas $\delta = 0.7$ is determined using more complete analysis (Ormes and Protheroe, 1983; Simon and Mathis, 1983). The $\delta = 0.5$ curve comes close to the lower limit on the scattering length given by setting the scattering length equal to the gyro radius, whereas the $\delta = 0.7$ curve stays at least a factor of 100 above that limit, even up to $10^8$ GV/c.

ORIGINAL PAGE IS
OF POOR QUALITY



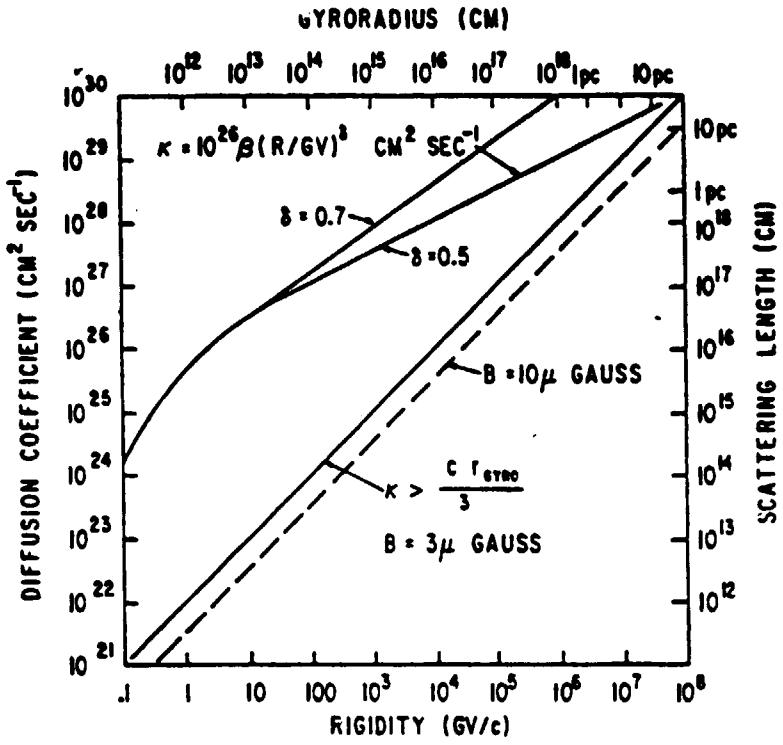


Fig. I. The assumed variation of the diffusion coefficient in interstellar space.

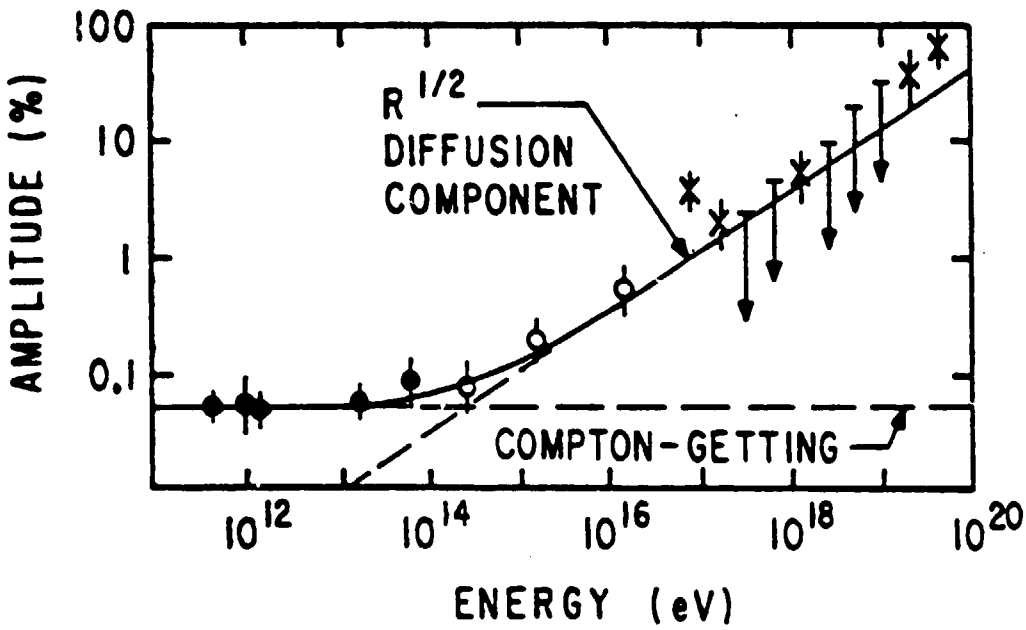


Fig. 2. The amplitude of the anisotropy is well fitted by a diffusion and a Compton-Getting component.

ORIGINAL PAGE IS
OF POOR QUALITY

(It is worth noting here that the escape length may not continue to decrease towards higher energy (see Chappell and Webber, 1981), in which case the connection between high (>10 GV/c) and low (<10 GV/c) energy regimes is not clear).

The anisotropy amplitude in the range $10^{12}$ to $10^{20}$ eV is shown in Figure 2. It is well fitted by two components: at energies below $10^{14}$ eV is a Compton-Getting anisotropy which corresponds to a streaming velocity of 20 km/sec and above is a diffusive anisotropy which comes from the cosmic rays flowing down the intensity gradient $\delta = \frac{3\kappa}{c} \frac{1}{N} \frac{dN}{dr}$ where N is the numer density and r is the spatial coordinate. A diffusion coefficient power law $\delta$ in the range 0.5 to 0.7 fits this data well.

Using the same diffusion coefficient at $10^6$ Gv/c and the anisotropy of $10^{-3}$ at $10^6$ GV/c, we can compute a half height for the intensity gradient of 1.5-15 kpc depending upon the value of $\delta$. These surely represent upper limits for the characteristic dimension of the storage volume because of the proximity of the solar system to the center of symmetry of the galactic disk.

From the time scale inferred from $^{10}$Be observations, we know that 1 GV/c nuclei have an age of about 10-20x$10^6$ yrs. (Wiedenback and Greiner, 1980 and Garcia-Munoz, Simpson and Wefel, 1981). Using this as a characteristic time, we see that with the small diffusion coefficient, 10 GV/c particles (4 GeV/nucleon) can only diffuse 100-200 pc from their sources whereas $10^6$ GV/c particles diffuse 3-10 kpc. It is unlikely then that there are more than one or two sources this close to the sun. The absence of a break in the high energy electron spectrum has been interpreted as saying that the nearest source must be within a few hundred parsec of the sun, but the spectrum of electrons is inconsistent with $\delta = 0.7$ and a standard leaky box picture. This problem may be resolved if the pathlength distribution is truncated due to the separation of the sun from this source. (See accompanying paper, Mauger and Ormes, 1983).

In summary then, we find that at low energies we are 100-300 pc from the nearest source, and that at higher energy the diffusive length is in the range of 1-10 kpc. These distance scales apply asuming that the diffusive medium has a characteristic size larger than these dimensions, and is the same everywhere throughout the volume. If the storage volume has smaller dimensions, then physical dimensions will be controlling, and the lifetime to reach that boundary will be inversely proportional to $\kappa$.

## 3. Conclusions

The relatively small distance which low energy particles (< 10 GV/c) can diffuse suggests that the roleover in the matter traversed below this energy (Garcia-Munoz et al., 1979 and Ormes and Protheroe, 1983) may be due to particles not yet having diffused to us from the nearest source. This is consistent with an increase in the truncation of the pathlength distribution at lower energies as reported by the Chicago group (Wefel et al. 1982).

ORIGINAL PAGE IS
OF POOR QUALITY

Such a small diffusion coefficient is consistent with the observation by Cane (1977) of 10-20 MHz radio emissivity on the line of sight to nearby HII regions. This data suggests there is a high emissivity region near the solar system. It would also imply the localization of particles to create point like gamma-ray sources. A prediction of this model would be that gamma-ray sources would be bigger at higher energy. Such an effect might be observable with the extended energy range and high sensitivity of the energetic gamma ray experiment (Fichtel et al., 1983) on the Gamma Ray Observatory.

The low energy cosmic rays would then have been confined very near the solar system, so that the observed grammage traversed and the $^{10}$Be abundance which lead to the conclusion that these cosmic rays have sampled a low density region of space $\rho = 0.3$ atoms/cm$^3$. This low density is consistent with the very local region of the galaxy where the sun may be inside a hot low density plasma or superbubble blown in the cold material of the average interstellar medium by repeated supernova explosions.

This picture leads to the following mix of sources. At low energy where the diffusion coefficient is small, each source is relatively isolated, and the composition we observe may be unique to that local source (and hence its general similarity to the solar system material). On the other hand at high energies in which our knowledge comes mostly from air shower observations, the diffusion coefficient is large, and we are bathed in the cosmic rays produced in a large number of sources, hence the low anisotropy values. There are no observations on the long term constancy of the cosmic ray intensity which rule out fluctuations on a time scale of $10^7$ years (Schaeffer 1977).

## 4. References

Cane, H. V., Ph.D Thesis, Non Thermal Background Radiation, 1977.
Chappell, J. H. and Webber, W. R., 17th ICRC, 2, 59, 1981.
Engelmann, J. J. et al., 17th ICRC, 9, 97, 1981.
Garcia-Munoz, M., Margolis, S. H., Simpson, J. A., and Wefel, J. P., 16th ICRC, 1, 310, 1979.
Garcia-Munoz, M., Simpson, J. A., and Wefel, J. P., 17th ICRC, 2, 72, 1981.
Garcia-Munoz, M., Guzik, T. G., Margolis, S. H., Simpson, J. A., and Wefel,, J. P., 17th ICRC, 9, 195, 1981.
Gregory, J. et al., 17th ICRC, 9, 154, 1981, and submittd to Phys. Rev. Letters.
Mauger, B. and Ormes, J. F., 18th ICRC, OG3-5, 1983
Ormes, J. F. and Protheroe, R. J., Ap. J. in press, 1983 and this this conference OG5.2-14.
Perron, C. et al., 17th ICRC, 9, 118, 1981.
Schaeffer, O. A., 14th ICRC, 11, 3508, 1975.
Simon, M. and Mathis, K. D., submitted to Astron. and Astrophys., 1983.
Streitmatter, R. E. and Balasubrahmanyan, V. K., private communication, 1983.
Wefel, J. D., Guzik, T. G., Garcia-Munoz, M., and Simpson, J. A., Bull. Am. Phys. Soc., 28, 743, 1983.
Wiedenbeck, M. E. and Greiner, D. E., Ap. J. 239, L139, 1980.

ORIGINAL PAGE IS
OF POOR QUALITY



# ACCELERATION AND PROPAGATION OF GALACTIC COSMIC RAYS: IMPLICATIONS OF HEAO-3 DATA

J.F. Ormes
NASA/Goddard Space Flight Centre, Greenbelt, Md 20771, U.S.A.

R.J. Protheroe
Dept. of Physics, University of Adelaide, South Australia 5001

ABSTRACT

We re-examine the energy dependence of the mean escape length of cosmic rays from the galaxy in the light of recent measurements of cosmic ray abundances from the Danish-French experiment on HEAO-3. Implications for cosmic ray acceleration and galactic confinement are discussed.

## 1. Introduction

Highly accurate data on the relative abundances of boron through nickel are now available from the Danish-French collaborative experiment (Bouffard et al., 1982) on HEAO-3. The boron to carbon ratio obtained from this experiment (Engelmann et al., 1981) is shown in Fig. 1 together with low energy observations from the IMP satellite (Garcia-Munoz et al., 1979). Balloon observations (original compilation by Garcia-Munoz et al., 1981a, with additions) are also shown to indicate the general agreement between these and the more accurate satellite data. We have used these results and performed a propagation calculation to determine the energy dependence of the mean escape length, $\lambda_e(E)$, from the observed secondary to primary ratios. Astrophysical implications of our result will be discussed. Full details of our analysis can be found in Ormes and Protheroe (1983).

## 2. Mean escape length

The method of calculation is as described by Protheroe et al. (1981). We have used source elemental abundances derived by Perron et al. (1982) and assumed source isotope ratios to be solar (Cameron, 1980), except for C, O, Ne, Mg, and Si for which we used those obtained by Wiedenbeck and Greiner (1981). For source abundances of the sub-iron group we have taken the local galactic abundances (Meyer, 1979). Energy dependent total cross sections of Letaw et al. (1982) were used. For spallation cross sections we have used the semi-empirical formulae of Silberberg and Tsao (1977) (see also Tsao and Silberberg, 1979 and references therein) except that those of iron have been normalized to measurements of Webber and Brautigam (1982) at 980 MeV/nuc.

First, we shall restrict our analysis to the high energy data (2.8-15 GeV/nuc) to probe the assymptotic behaviour of $\lambda_e$, avoiding biases introduced at low energies by solar modulation effects, strong energy dependence of cross sections, and velocity dependent propagation effects. For a source spectrum appropriate to acceleration by strong shocks, i.e. $dJ/dT \propto p^{-2}$, we have calculated the secondary to primary ratios for two possible forms of the energy variation of $\lambda_e$: (a) a power law in rigidity; (b) a power law in kinetic energy. We show in Figure 2 the results of a comparison of our calculations with three important secondary to primary ratios obtained from the HEAO-3 data for the two forms of $\lambda_e$ (the equations used are given in the figure). The results are given in the form of a $\chi^2$ contour plot in the $\Lambda$-$\delta$ plane. For

ORIGINAL PAGE IS
OF POOR QUALITY



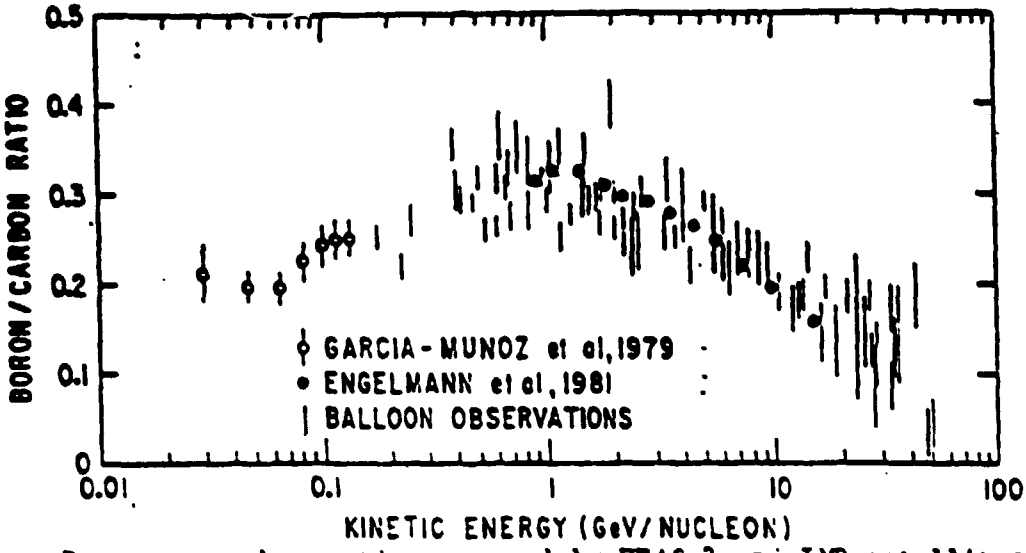


Figure 1 Boron to carbon ratio measured by HEAO-3 and IMP satellites compared with a survey of balloon observations.

clarity, only the contour corresponding to the 95% confidence interval has been plotted. It is clear that for the B/C, N/O, and Sc-Mn/Fe ratios, the HEAO data give a best value of $\delta$ somewhat higher then previously realized. We find $\delta_R = 0.7 \pm 0.1$ for the rigidity dependent fit and $\delta_T = 0.63 \pm 0.1$ for the kinetic energy per nucleon dependent fit.

Previous estimates based on balloon data placed $\delta_T$ in the range of 0.3-0.5, however Perron et al. (1981) in their analysis of the HEAO data suggested larger values of $\delta$ would fit better. If one were to ignore the quoted errors on the HEAO data and include data at lower energies in the fit, lower values of $\delta_T$ would be obtained. Also, kinematic effects make $\delta_R$ larger than $\delta_T$ in this energy range.

From Figure 2, we find that the best value of $\Lambda$ obtained from the ratio of iron-secondaries to iron is about 10% higher than that obtained from the boron to carbon ratio. This is consistent with a slightly truncated pathlength distribution, for example as expected in the nested leaky box model (Cowsik and Wilson, 1973) and would imply about 8% of $\lambda_e$ could be in source regions. Unfortunately, this conclusion cannot be reached because of systematic uncertainties in spallation cross sections of order 10%. To illustrate this point the acceptable range of $\Lambda_R$, obtained from the boron to carbon data allowing for a 10% uncertainty in the partial cross sections, has been added to Figure 3(a) and includes the region between the two dashed lines. The 'best' values of $\Lambda_R$ obtained from the three secondary to primary ratios shown in Figure 3(a) then appear to be entirely consistent. For further discussion of truncated pathlength distributions, see Protheroe et al. (1981) and Garcia-Munoz et al. (1981a).

We show in Figure 3 the mean escape length we derive from the boron to carbon ratio results from the HEAO-3 and IMP experiments. For this, we have assumed that the solar modulation can be described by the force field approximation with a deceleration parameter, $\phi$, of 600 MV appropriate to near solar maximum conditions (Urch and Gleeson, 1973). We show (dashed line) $\lambda_e = 35\ (R/GV/c)^{-0.7}$ g/cm$^2$ we obtained for data above 2.8 GeV/nuc. Clearly, this gives a poor fit to the low energy data. Satisfactory agreement with the data is obtained (solid line) with,

ORIGINAL PAGE IS
OF POOR QUALITY



$$\lambda_e = 35 \left\{1 + \left(\frac{1.88\ GV/c}{R}\right)^2\right\}^{-1.5} \left(\frac{R}{GV/c}\right)^{-0.7}\ g/cm^2 \qquad (1).$$

The turnover in $\lambda_e$ at low energies is considerably more abrupt than can be accounted for by the Dynamical Halo model (see e.g. Jones, 1979).

## 3. Discussion

At high energies, the variation of $\lambda_e$ with energy may be as steep as $R^{-0.7}$. Since the observed spectra of primary nuclei (e.g. Ryan et al. 1972) are proportional to $R^{-2.7}$, this would imply that primary cosmic rays may be produced with a $p^{-2}$ spectrum as expected for acceleration by a first order Fermi mechanism in strong shocks (compression ratio 4, or certainly greater than 3.5; see e.g. Axford, 1981).

As well as implications for the acceleration of cosmic rays, the steep rigidity dependence of $\lambda_e$ has important consequences regarding the distance cosmic rays propagate (the cosmic ray age must be greater than the speed of light crossing time of the storage volume). Since there is no observed structure (e.g., change of slope) in the proton spectrum up to $10^5$ GV/c (Gregory et al., 1981, Tasaka et al., 1982), we conclude that the rapid decrease of $\lambda_e$ continues up to this rigidity. We shall assume that the lifetime of cosmic rays is proportional to $\lambda_e$. Extrapolating from $\sim 10^7$ y at 1 GV/c (Wiedenbeck and Greiner, 1980; Garcia-Munoz et al., 1981b) using equation (1), the age at $10^5$ GV/c is $\sim$ 4000y and the size of the "storage region" must be less than 1 kpc. Particles which propagate diffusively must strongly satisfy this inequality.

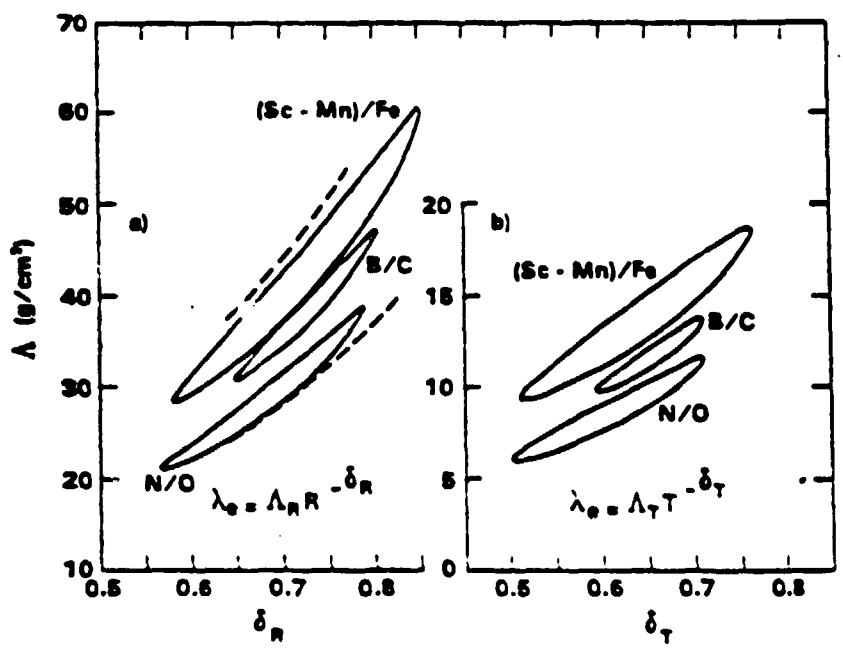


Figure 2 Comparison of boron to carbon, sub-iron to iron, and nitrogen to oxygen ratios observed from 2.8-15 GeV/nuc by HEAO-3 with results of the present propagation calculations. The figure shows the goodness of fit when $\Lambda_R$ and $\delta_R$ (part a) or $\Lambda_T$ and $\delta_T$ (part b) are varied. The closed curves are contours of constant $\chi^2$ corresponding to 95% probability.

ORIGINAL PAGE IS
OF POOR QUALITY



Part of this work was performed as a HEAO-3 guest investigation. J.F. Ormes would like to thank Drs. L. Koch-Miramond and N. Lund for their hospitality and discussions during visits to Saclay and DSRI in 1981. We are grateful to Drs. S.A. Stephens, V.K. Balasubrahmanyan and M. Simon for useful discussions.

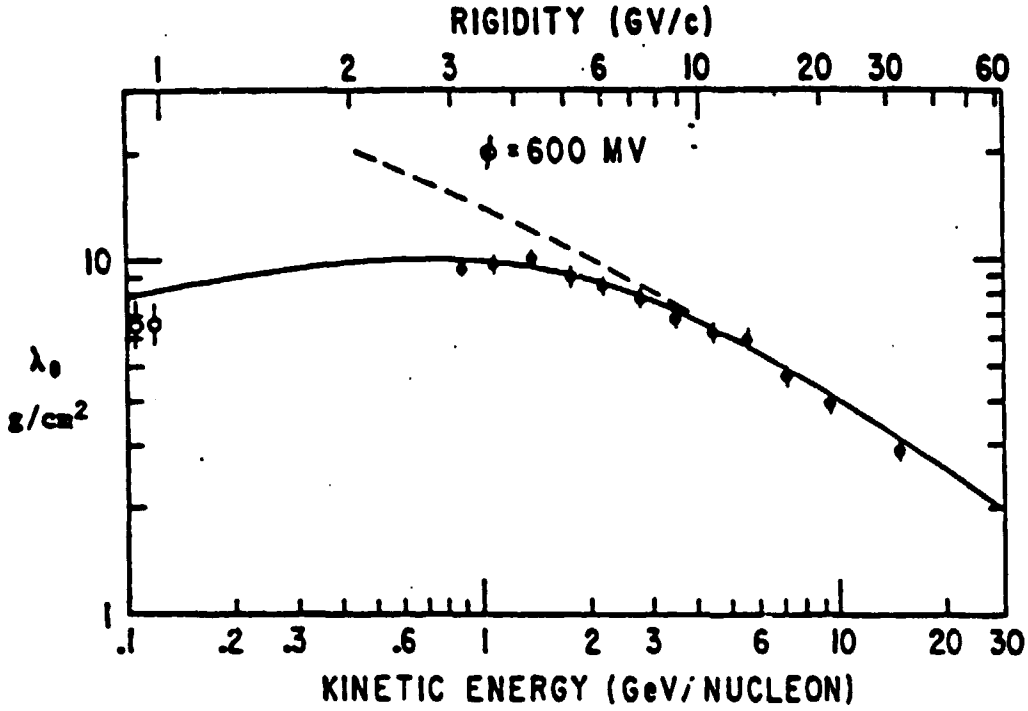


Figure 3 Mean escape length derived by us from HEAO-3 and IMP measurements of the boron/carbon ratio. Dashed curve shows assymptotic behaviour; solid line is the fit given in equation (1).

**References**

Axford, W.I., 1981, Proc. 17th ICRC, 12, 155.
Bouffard, M., et al., 1982, Ap. and Sp. Sci., 84, 3.
Cowsik, R. and Wilson, L.W. 1973, Proc. 13th ICRC, 1, 500.
Engelmann, J.J., et al., 1981, 17th ICRC, 9, 97.
Garcia-Munoz, M., et al., 1979, 16th ICRC, 1, 310.
Garcia-Munoz, M. 1981a, Proc. 17th ICRC, 2, 192.
Garcia-Munoz, M., et al., 1981b, Proc. 17th ICRC, 2, 72.
Gregory, J.C., et al., 1981, Proc. 17th ICRC, 9, 154.
Jones, F.C., 1979, Ap. J. 229, 747.
Letaw, J.R., Silberberg, R., Tsao, C.H., 1982, Ap. J. Suppl. (in press).
Meyer, J.P., 1979, 16th ICRC, 2, 115.
Ormes, J.F. and Protheroe, R.J., 1983, Ap. J., September 15 issue.
Perron, C., et al., 1981, Proc. 17th ICRC, 9, 118.
Protheroe, R.J., et al., 1981, Ap. J. 247, 362.
Ryan, M.J., et al., 1972, Phys. Rev. Lett., 28, 985.
Silberberg, R. and Tsao, C.H. 19--, Ap. J. Suppl., 35, 129.
Tasaka, S., et al., 1982, Phys. Rev. D25, 1765.
Tsao, C.H., and Silberberg, R., 1979, Proc. 16th ICRC, 2, 202.
Urch, J.H. and Gleeson, L.J., 1973, Ap. Space Sci., 20, 117.
Webber, W.R. and Brautigam, 1982, Ap. J. 260, 894.
Wiedenbeck, M.E. and Greiner, D.E., 1980, Ap. J. 239, L139.

ORIGINAL PAGE IS
OF POOR QUALITY



# HOW DO COSMIC RAYS CHANGE THEIR ENERGY IN THE SOLAR WIND?

Frank C. Jones
Laboratory for High Energy Astrophysics
NASA/Goddard Space Flight Center
Greenbelt, Maryland 20771
USA

## ABSTRACT

We have derived the diffusion-convection (modulation) equation directly from the Boltzman equation employing a minimum number of assumptions about the scattering process. We assume that each scatterer has a reference frame in which 1) the scattered particles undergo no change in energy, and 2) isotropy is an equilibrium state. If the background plasma contains a magnetic field and the flow speeds of the plasma and scattering centers are different additional terms arise that modify the usual equations. Furthermore if the scatterers have individual motions relative to their average flow the second order Fermi acceleration term appears.

## 1. Introduction

The diffusion-convection equation was first applied to cosmic-ray modulation by parker (1965,1966). Gleeson and Axford (1967) were the first to derive it from the more general Boltzmann equation:

$$\frac{\partial f}{\partial t} + \vec{v} \cdot \vec{\nabla} f + \vec{F} \cdot \vec{\nabla}_p f = \frac{\partial f}{\partial t}\Big)_c \qquad (1)$$

where the left hand side of the equation represents the streaming of the particles through the large scale, average force fields represented by $\vec{F}$ and the right hand side represents the change in the distribution function f due to stochastic forces or scattering. In their paper Gleeson and Axford did not include any large scale magnetic or electric fields and treated the scattering as hard sphere scattering. If one considers a magnetic field embedded in a plasma flowing with a velocity $\vec{V}_p$ one must include both the magnetic and induced electric fields in the force term,

$$\vec{F} = \frac{\vec{P} \times \vec{\omega}}{\gamma} - m\,\vec{V}_p \times \vec{\omega} = (\vec{P} - m\gamma\,\vec{V}_p) \times (\frac{\vec{\omega}}{\gamma}) \qquad (2)$$

where $\vec{p}$ is the particle momentum, m is the particle mass, $\gamma$ is the particles Lorentz factor, $\vec{V}_p$ is the plasma flow velocity and $\vec{\omega} = e\vec{B}/mc$, the particles local gyrofrequency.

ORIGINAL PAGE IS
OF POOR QUALITY



## 2. The Collision Term

We may calculate the collision term in the manner of Gleeson and Axford by performing the calculation in the rest frame of an individual scattering center. In this frame we make two important assumptions namely: the scattered particles do not change their energy in a single scattering and the scattering process is such that it will preserve isotropy. We further assume that the momentum transfer, averaged over the cross section, may be written as a tensor operating on the original momentum.

It should be noted that we assume nothing about the strength of the scattering; it could be strong as in hard sphere scattering or weak as in scattering by weak Alfven waves.

## 3. The Transport Equation

The transport equation is obtained by the usual weakly anisotropic expansion. it is assumed that the distribution function may be described by its first two moments:

$$f(\vec{p}, \vec{x}) = \frac{1}{4\pi} n(p,\vec{x}) + \frac{3}{4\pi} \vec{\phi}(p,\vec{x})\cdot\hat{P} \tag{3}$$

where $n(p,\vec{x}) = \int d\hat{p} f(\vec{p},\vec{x})$

and $\vec{\phi}(p,\vec{x}) = \int d\hat{p}\ \hat{p}\ f(\vec{p},\vec{x}).$ (4)

If the scattering centers have a mean velocity $\vec{V}_s$ and have a dispersion about this mean $\langle\delta\vec{V}_s\rangle$ we obtain after a great deal of coordinate transformations, integrations and algebra the following transport equation:

$$\begin{aligned}
&\frac{\partial n}{\partial t} - \vec{v}\cdot\overleftrightarrow{K}\cdot\vec{\nabla}n - \frac{1}{3}(\vec{v}\cdot\vec{V}_p)\, p\,\frac{\partial n}{\partial p} + \vec{V}_p\cdot\vec{\nabla}n \\
&= -\frac{1}{3} p\vec{\nabla}\cdot\left[(\overleftrightarrow{\Omega}+\overleftrightarrow{\nu})^{-1}\cdot\overleftrightarrow{\nu}\cdot\Delta\vec{V}\frac{\partial n}{\partial p}\right] + \frac{1}{3} p\,\Delta\vec{V}\cdot\nu\cdot(\overleftrightarrow{\Omega}+\overleftrightarrow{\nu})^{-1}\cdot\left(\frac{\partial}{\partial p}\vec{\nabla}n\right) \\
&+ \frac{1}{3}\Delta\vec{V}\cdot\overleftrightarrow{\nu}\cdot(\overleftrightarrow{\Omega}+\overleftrightarrow{\nu})^{-1}\cdot\left[4 - \overleftrightarrow{\nu}\cdot(\overleftrightarrow{\Omega}+\overleftrightarrow{\nu})^{-1}\right]\cdot\vec{\nabla}n \\
&+ \Delta\vec{V}\cdot\overleftrightarrow{\nu}\cdot(\overleftrightarrow{\Omega}+\overleftrightarrow{\nu})^{-1}\cdot\overleftrightarrow{\Omega}\cdot\Delta\vec{V}\frac{m\gamma}{3p}\frac{\partial}{\partial p}\left(m\gamma p\frac{\partial n}{\partial p}\right) \\
&- (\vec{V}_p\cdot\overleftrightarrow{\Omega}\vec{V}_s + \overleftrightarrow{\nu})\cdot(\overleftrightarrow{\Omega}+\overleftrightarrow{\nu})^{-1}\cdot\overleftrightarrow{\nu}\cdot(\overleftrightarrow{\Omega}+\overleftrightarrow{\nu})^{-1}\cdot\overleftrightarrow{\Omega}\cdot\Delta\vec{V}\frac{\partial n}{\partial p} \\
&\frac{1}{3}\frac{m\gamma}{p^3}\langle\delta\vec{V}_s\cdot\overleftrightarrow{\nu}\cdot\delta\vec{V}_s\rangle\frac{\partial}{\partial p}\left(m\gamma p^3\frac{\partial n}{\partial p}\right)
\end{aligned} \tag{5}$$

In the above equation $\overleftrightarrow{K}$ is the diffusion tensor given by

$$\overleftrightarrow{K} \equiv \frac{1}{3}\left(\frac{p}{m\gamma}\right)^2(\overleftrightarrow{\Omega}+\overleftrightarrow{\nu})^{-1}$$

ORIGINAL PAGE IS
OF POOR QUALITY



where $\bar{\bar{\nu}}$ is the scattering tensor whose elements are the various scattering frequencies and $\bar{\bar{\Omega}}$ is the gyro frequency tensor defined by $\bar{\bar{\Omega}} \cdot \vec{V} = \vec{\omega} \times \vec{V}/\gamma$. It should be noted that inclusion of $\bar{\bar{\Omega}}$ in the diffusion tensor produces gradient and curvature drifts of the particles. $\Delta\vec{V}$ is the difference between the plasma and scattering center velocities, $\Delta\vec{V} = \vec{V}_p - \vec{V}_s$ and the last term on the right hand side is the Fermi acceleration term and is zero if the scattering centers all move with a single velocity, i.e., $\delta\vec{V}_s = 0$.

## 4. Conclusions

Two things should be noted about equation (5): first, if the scattering frequency is small compared to the gyro-frequency ($\bar{\bar{\nu}} \ll \bar{\bar{\Omega}}$), as is usually the case, all of the terms on the right hand side (RHS) are small and may be neglected (with the possible exception of the Fermi term); second, the velocity that appears in the left hand side (LHS) (the usual modulation equation) is the plasma velocity not the scattering center velocity. If we consider the reverse limit, $\bar{\bar{\Omega}} \ll \bar{\bar{\nu}}$ the first three terms on the RHS are of order unity and have the effect of replacing $\vec{V}_p$ with $\vec{V}_s$ on the LHS. The remaining terms on the RHS are small in this limit too and are only of interest in the intermediate region $\vec{\Omega} \cdot \vec{B} = 0$ and the scattering center motion is the approriate one to use.

In the directions perpendicular to $\vec{B}$, however, the modulation equation should use the plasma velocity and, in most cases, it is not the motion of the scattering centers that sweeps the cosmic rays out of the solar cavity but the $\vec{E} \times \vec{B}$ drift instead.

## 5. References

Parker, Ea. N., (1965), Planet. Space Sci., 13, 9
, (1966) ibid., 14, 371
Gleeson, L. J. and Axford, W. I., (1967), Ap. J., 149, L115

ORIGINAL PAGE IS
OF POOR QUALITY



# SOLAR $^3$HE-RICH EVENTS OBSERVED ON ISEE-3

D. V. Reames, and T. T. von Rosenvinge
NASA/Goddard Space Flight Center, Greenbelt, MD 20771, U.S.A.

ABSTRACT

A scan has been made of ISEE-3 data for all events with $^3He/^4He > 0.20$ at > 1.3 MeV/nucl. The 67 events found show some evidence of 27-day recurrence. Larger events show both velocity dispersion and magnetic field-aligned arrival from the solar direction. At least one third of the events are preceded by increases in ~ 300 keV electrons, although several larger events show no electron increases. $^3$He spike events also exist suggesting nearly scatter-free propagation of $^3$He from well-connected events.

## 1. Introduction

Despite a decade of observation (see Ramaty et al., 1980), our understanding of $^3$He-rich solar particle events and of the conditions under which they occur remains qualitative at best. In this paper we describe some results of a survey of approximately 4 years of ISEE-3 data that seeks to characterize these events more completely.

Earlier papers (von Rosenvinge and Reames, 1979; Reames and von Rosenvinge, 1981) described the ISEE-3 very low-energy telescope (VLET) and showed examples of the element and isotope resolution it provides.

## 2. Data Analyses and Results

The survey was performed using the 1.3-1.6 MeV/nucl and 2.2-3.1 MeV/nucl $^3$He and $^4$He fluxes in 6-hour averaged intervals from August 15, 1978 through June 10, 1982. A $^3$He-rich interval was defined when either or both of the energy intervals met the following two criteria:

1) The error in the $^3$He flux from all sources was less than 50 percent

2) The $^3He/^4He$ ratio was > 0.20 (when the $^4$He flux was zero the ratio was defined as the number of $^3$He particles in the interval).

A candidate $^3$He event consisted of at least two successive $^3$He-rich intervals. These events were then observed at a higher time resolution to identify multiple events, to account for data-gap effects and to better define the onset times.

Of 5,628 intervals with data, 300 were $^3$He-rich and 67 event periods were identified. This amounts to a 5.3 percent probability of a

ORIGINAL PAGE IS
OF POOR QUALITY



$^3$He-rich event in progress or an average event rate of one every 3 weeks during this period of the solar cycle.

The time distribution of the events is shown on a 27-day Bartels-rotation plot in Figure 1. Recurrences seen in the figure exceed those expected from a random distribution and suggest the recurrence of events from the same solar active region. It has not yet been possible to associate many of the small $^3$He events with solar flares to establish their origin.

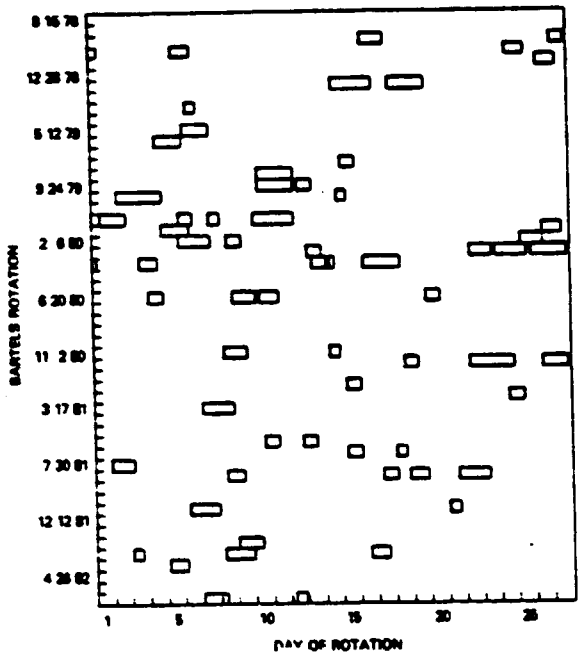


Fig. 1 27-day recurrence plot of $^3$He-rich event times.

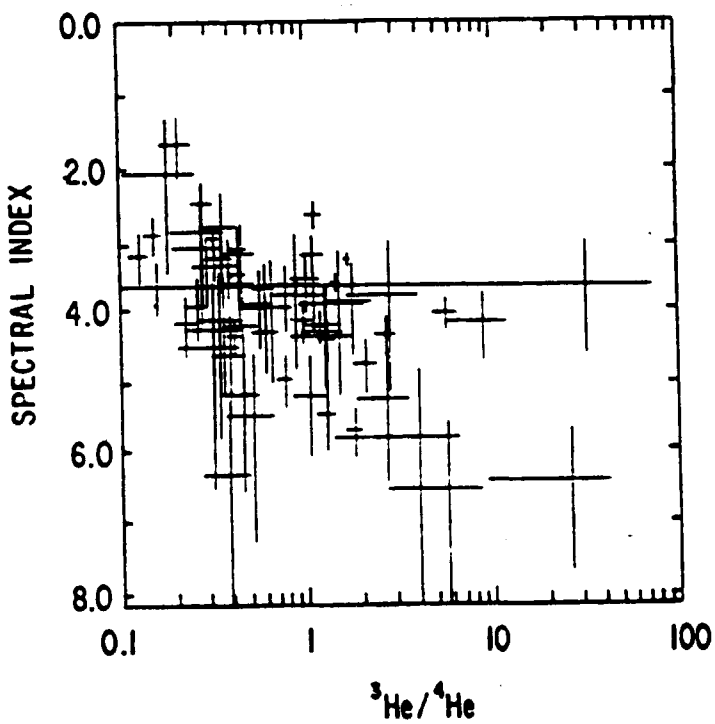


Fig. 2 Scatter plot of event-averaged $^3$He spectral index versus $^3$He/$^4$He ratio.

ORIGINAL PAGE IS
OF POOR QUALITY



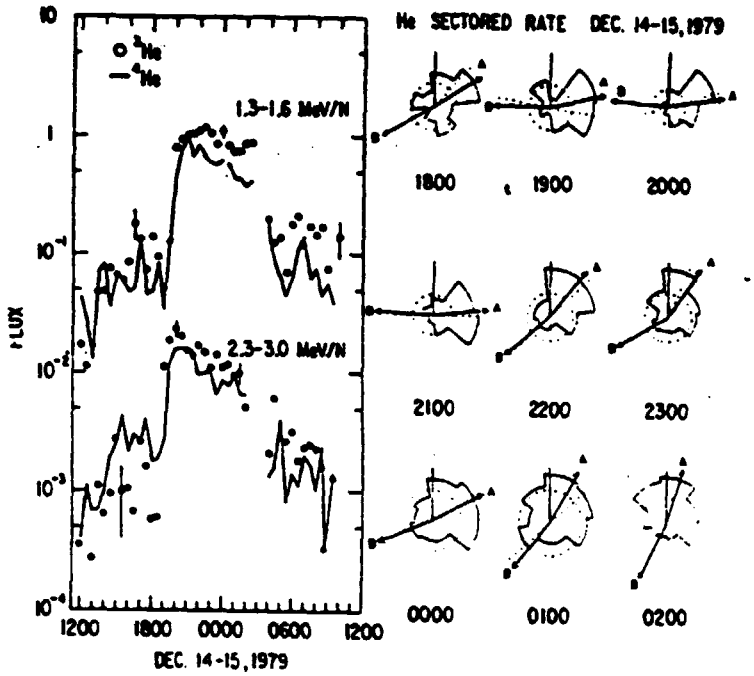


Fig. 3 Time histories of $^3$He and $^4$He and He sectored rate plots. The direction of the Sun is at the top and A and B are the aniso tropy and magnetic field directions.

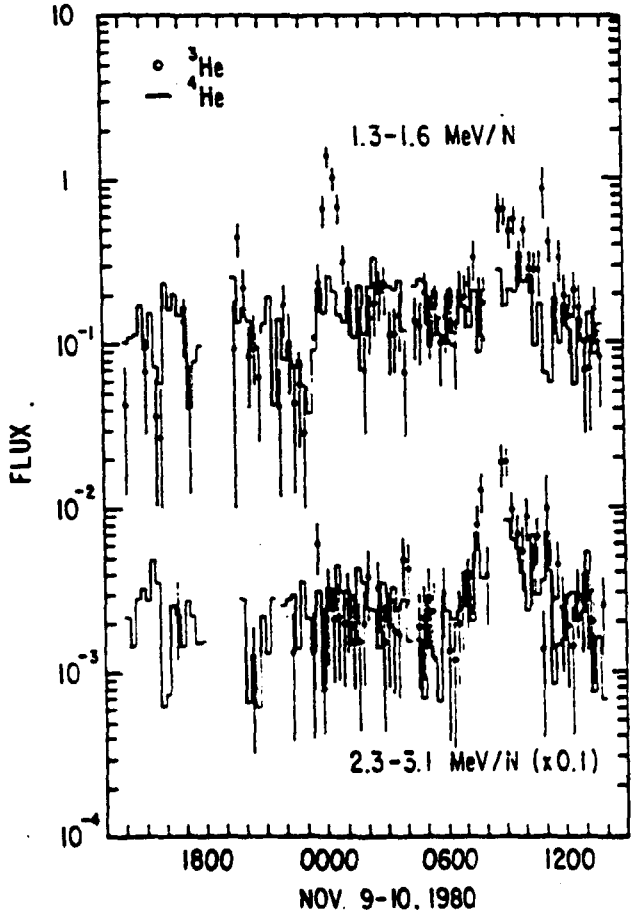


Fig. 4 $^3$He spike increases during the 11/9/80 event.

ORIGINAL PAGE IS
OF POOR QUALITY



Another new feature found in the survey data and shown in Figure 2 is the tendency of events with large $^3He/^4He$ ratios to have steeper spectra.

## 3. Time Histories

A different aspect of the $^3He$-event characterization may be seen from the time histories as shown in Figure 3 for the largest event in the survey. This event typifies two frequently observed features of $^3He$ events, namely: 1) velocity dispersion (earlier arrival of higher velocity particles) and 2) large and persistent field-aligned anisotropies. A third feature of the events is an absence of correlation with interplanetary shocks, sector boundaries or $^3He$ abundance in the solar wind. These features establish that the events are indeed solar in origin.

Further evidence of velocity dispersion is shown in about one-third of the events that have clearly associated increases of > 300 keV electrons preceding the event by 1 to 12 hours. Electron increases are not observed in all events however.

Figure 4 shows an extreme example of fast spike increases in $^3He$ that are seen in some events. The increase at 0 hours on November 10 shows strongly field-aligned flow of $^3He$. R. Zwickl (1983) has informed us that a "Strahl" involving field-aligned electron flows described by Rosenbauer (1976) is in progress during this period. Efficient "scatter-free" propagation of $^3He$ from an impulsive solar event along well-connected field lines could explain the fast profile observed.

## References

Reames, D. V. and T. T. von Rosenvinge, 1981, 17th Conf. Papers 3, 162.
Ramaty, R., et al., 1980 in Solar Flares, P. Sturrock ed., Colo. Assoc.Univ. Press.
Rosenbauer, H., et al., 1976, Symposium on Solar-Terrestrial Physics, p 312, Am. Geophys. Union.
von Rosenvinge, T. T., and D. V. Reames, 1979, 16th Conf. Papers 5, 68.
Zwickl, R., 1983, Los Alamos National Lab., personal communication.

ORIGINAL PAGE IS
OF POOR QUALITY



# SOLAR FLARE NEUTRONS AND GAMMA RAY LINES

R. E. Lingenfelter
University of California, San Diego, CA, 92093, U.S.A.

R. Ramaty and R. J. Murphy[1]
NASA/Goddard Space Flight Center, Greenbelt, MD 20771, U.S.A.

B. Kozlovsky
Tel Aviv University, Israel

## ABSTRACT

We have derived the energy spectrum of accelerated protons and nuclei at the site of the June 21, 1980 limb flare by a new technique, using observations of the time-dependent flux of high-energy neutrons at the Earth. We find that this energy spectrum is very similar to the energy spectra of 7 disk flares for which the accelerated particle spectra have been previously derived using observations of 4-7 MeV to 2.223 MeV fluence ratios.

## 1. INTRODUCTION

High energy neutrons, produced by nuclear reactions of flare-accelerated protons and nuclei, were recently discovered from solar flares with detectors on the SMM (Chupp et al., 1982). The observed time dependence of the neutron flux at Earth gives a time-of-flight measurement of the neutron energy spectrum at the Sun, provided that the duration of the flare is much shorter than the typical Sun-Earth neutron transit time (~ 10 minutes). Calculations of neutron energy spectra produced in solar flares and predictions of the expected time dependences of the neutron flux at Earth were made previously (Lingenfelter et al., 1965; Lingenfelter and Ramaty, 1967). The time profile of the neutron flux observed (Chupp et al., 1982; E. L. Chupp, private communication 1983) from the June 21, 1980 flare is consistent with these predictions. Comparison of the observed time dependence with such calculations allows us to determine the energy spectrum and total number of the accelerated particles at the site of the flare.

Neutron production in solar flares is accompanied by the production of nuclear gamma radiation (Lingenfelter and Ramaty, 1967; Ramaty, Kozlovsky and Lingenfelter, 1975). Comparisons (Ramaty, 1983) of the relative intensities of gamma-ray lines from flares (e.g., Chupp, 1982) with calculated line ratios provide independent information on the number and spectrum of flare-accelerated particles.

Comparisons of gamma-ray observations from flares and charged-particle measurements in the interplanetary medium have shown (e.g., von

[1]Also University of Maryland, College Park, MD 20742, U.S.A.

Rosenvinge, Ramaty and Reames, 1981) that gamma-ray production in solar flares takes place predominantly during the slowing-down of the accelerated particles in the solar atmosphere, rather than during their acceleration or escape from the Sun. This is reasonable since particle acceleration generally requires a low ambient density so that the acceleration rate exceeds the energy-loss rate, whereas effective nuclear interactions require an ambient density that is high enough to stop the particles. Thus, we expect the region of most efficient acceleration to be above the interaction region where the observed neutrons and gamma rays are produced. This model of nuclear interactions is commonly referred to as the thick-target model.

We have recently (Ramaty et al., 1983) carried out new thick-target calculations of neutron production in solar flares. Here we briefly describe these calculations; we compare them to the high-energy neutron observations of the June 21, 1980 limb flare; and we derive the energy spectrum and number of the protons and nuclei accelerated in this flare. Then by deriving the fluences of the accompanying nuclear gamma radiation, we confirm that, for limb flares, the 2.223 MeV line from neutron capture on $^1H$ is strongly attenuated by Compton scattering in the photosphere (Wang and Ramaty, 1974; Chupp, 1982).

The spectrum of the accelerated protons and nuclei has also been derived from observations of the 4-7MeV-to-2.223MeV fluence ratio for disk flares. We find that the proton spectra obtained previously (Ramaty 1983) for 7 disk flares using this method are very similar to the proton spectrum derived using high energy neutron observations for the June 21, 1980 limb flare, showing that flares which produce detectable high energy neutron fluxes do not appear to be significantly different from other flares observed on the disk.

## II. PRODUCTION OF HIGH ENERGY NEUTRONS

The calculations presented here are performed using the thick-target model. We take the energy spectrum of the protons and nuclei that emerge from the acceleration region and are incident on the interaction region to be the Bessel function appropriate for stochastic Fermi acceleration, $N(E) \propto K_2[2(3p/(mc\alpha T))^{1/2}]$ (Ramaty 1979). The product $\alpha T$ characterizes the particle spectrum, such that a larger value of $\alpha T$ corresponds to a harder spectrum. The above form for N(E) is valid for nonrelativistic energies and an energy-independent $\alpha T$. We assume, in addition, that the composition of the accelerated particles is the same as that of the solar atmosphere and that the protons and nuclei have the same energy spectrum. These particles are then allowed to slow down in the interaction region due to ionization losses in a neutral medium. For simplicity, we also assume that within the interaction region the angular distribution of the charged particles is isotropic. An anisotropic distribution would have observable effects. For example, if the protons and nuclei were preferentially directed downward toward the photosphere, the neutron flux from a limb flare would be larger than from a disk flare. There is, however, no data as yet to suggest such an anisotropy.

ORIGINAL PAGE IS
OF POOR QUALITY



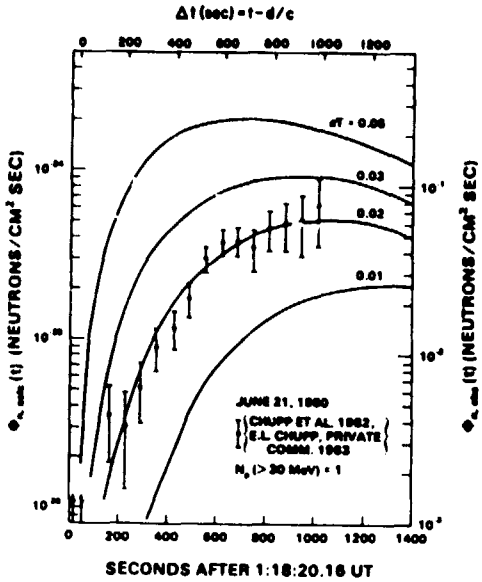


Figure 1. Observed and calculated neutron fluxes at Earth as functions of the difference between the Sun-Earth transit times of neutrons and photons; we take d/c=500 sec.

The calculated time-dependent neutron fluxes at the Earth are shown in Figure 1 for various values of $\alpha T$, assuming instantaneous production and free, unattenuated escape from the Sun. The time $\Delta t$ is that in excess of the light travel time from the Sun, where t is measured from the neutron production time. Also shown in this figure is the observed neutron flux from the June 21, 1980 flare (Chupp et al. 1982; E. L. Chupp, private communication 1983). We assumed that the neutron production time was at 1:18:55 UT - d/c, i.e. at the midpoint between the two impulsive photon emission peaks whose centers, shown by arrows, were observed at 1:18:40 and 1:19:10 UT (e.g. Chupp et al. 1982). The total duration of the impulsive phase of the June 21, 1980 flare was ~ 60 sec. As can be seen, the shape of the observed time dependence fits very well that calculated for $\alpha T$=0.02. The absolute normalization of the data to the calculations implies a total production of 2.8 x $10^{30}$ neutrons and a total number of accelerated protons with energies greater than 30 MeV, $N_p(>30\text{MeV}) \simeq 1.2\times10^{33}$.

The assumption of free neutron escape limits the maximum ambient density in the interaction region. If the dependence on height of the ambient density in the interaction region can be approximated by an exponential with scale height $h_o$, $n(h) \propto \exp(-h/h_o)$, then for a limb flare, the observable neutron flux originating at a height h is attenuated by $\sim \exp\left[-((\pi/2)Rh_o)^{1/2}\sigma_{np}\, n(h)\right]$, where R is the solar radius and $\sigma_{np}$ is the neutron-proton elastic scattering cross section. Since $\sigma_{np}$ increases with decreasing neutron energy, the maximum value of n(h) consistent with free neutron escape is determined by the lowest observed neutron energy, ~50MeV (Chupp et al. 1982). For $h_o \simeq 10^7$cm, we find that $n \lesssim 5\times10^{15}$ cm$^{-3}$, essentially the top of the photosphere. Since the vertical column depth at this density is only ~ 0.2 gm/cm$^2$ (Vernazza, Avrett and Loeser 1981), while the stopping ranges of the protons that produce the neutrons are >5 gm/cm$^2$, the protons must be stopped at column depths significantly less than their ranges, perhaps by magnetic mirroring (Zweibel and Haber 1983) or by scattering from magnetic inhomogeneities.

Lastly, we consider the 2.223 MeV gamma-ray line resulting from the production of neutrons in the June 21, 1980 flare. Calculations (Wang and Ramaty 1974) of neutron slowing down and capture on $^1$H predict that

ORIGINAL PAGE IS
OF POOR QUALITY



there will be a strong limb darkening of the resultant 2.223 MeV line owing to Compton scattering in the photosphere. Taking the estimated (Ramaty 1983) value of 0.23 for the number of observable 2.223 MeV photons per neutron from a disk-centered flare, the total production of $2.8 \times 10^{30}$ neutrons implies a 2.223 MeV line fluence of ~230 photons/cm$^2$ at the Earth from such a flare. The fact that the observed (Chupp 1982; D. Forest, private communication 1982) 2.223 MeV line fluence for the June 21, 1980 limb flare was only ~6 photons/cm$^2$, provides clear evidence for the limb-darkening of this line.

## ACKNOWLEDGEMENTS

We wish to thank E. L. Chupp and D. J. Forrest for providing data prior to publication. Financial support for these studies came from NASA through the Solar Terrestrial Theory Program and from the NSF through the Solar Terrestrial Program.

## REFERENCES

Chupp, E. L. 1982, in Gamma-Ray Transients and Related Astrophysical Phenomena, ed. R. E. Lingenfelter, et al., (NY: AIP), p. 363.

Chupp, E. L. et al. 1982, Ap. J. (Letters), 263, L95.

Lingenfelter, R. E., et al. 1965, J. Geophys. Res., 70, 4077, 4087.

Lingenfelter, R. E. and Ramaty, R. 1967, in High Energy Nuclear Reactions in Astrophysics, ed. B.S.P. Shen (NY: W. A. Benjamin), p. 99.

Ramaty, R. 1979, in Particle Acceleration Mechanisms in Astrophysics, ed. J. Arons et al. (NY: AIP), p. 135.

Ramaty, R. 1983, in The Physics of the Sun, ed. P. A. Sturrock et al., in press

Ramaty, R. Kozlovsky, B., and Lingenfelter, R. E. 1975, Space Sci. Rev., 18, 341.

Ramaty, R. et al. 1983, Solar Phys., in press.

Vernazza, J. E., Avrett, E. H., and Loeser, R. 1981, Ap. J. Supl., 45, 635.

von Rosenvinge, T. T., Ramaty, R. and Reames, D. V. 1981, 17th Intl. Cosmic Ray Cnf. Papers, Paris, 3, 28.

Wang, H. T., and Ramaty, R. 1974, Solar Phys., 36, 129.

Zweibel, E. G. and Haber, D. 1982, Ap. J., 264, 648.

ORIGINAL PAGE IS
OF POOR QUALITY



# THE GSFC ADVANCED COMPTON TELESCOPE (ACT)

R. Hartman, C. Fichtel,
D. Kniffen, G. Stacy[1], J. Trombka
NASA/Goddard Space Flight Center
Greenbelt, MD 20771

ABSTRACT

A new telescope is being developed at GSFC for the study of point sources of gamma rays in the energy range 1-30 MeV. Using the detection principle of a Compton scatter in a 2.5 cm thick NaI(Tℓ) detector followed by absorption in a 15 cm thick NaI(Tℓ) detector, the telescope uses a rocking collimator for field-of-view reduction and background subtraction. Background reduction techniques include lead-plastic scintillator shielding, pulse shape discrimination and Anger camera operation in both NaI detectors, as well as a time-of-flight measurement between them. The instrument configuration and status will be described.

## 1. Introduction

There is particular interest in the study of "medium energy" cosmic γ rays for a variety of reasons. This energy regime (from a few hundred keV to approximately 30 MeV) constitutes a transition region from relatively low energy thermal processes to highly energetic non-thermal astrophysical phenomena (e.g., nuclear radiation, $\pi^0$ decays, inverse Compton). For a variety of both galactic and extragalactic objects (supernovae, neutron stars, active galaxies), various models predict peak power of emitted radiation in the medium energy γ-ray region. In addition, observations of the diffuse γ-ray background emission appear to indicate that there may be inflections in the energy spectrum of that emission in the few MeV region. Such a break in the energy spectrum of the γ-ray background could contain important cosmological information on the history and evolution of the Universe.

To date, there have been few confirmed detections in the medium energy γ-ray region. Most experiments have yielded only upper limits. The major problem is that in this energy region one encounters low fluxes and relatively high levels of instrumental background; in addition, separation of point sources from the diffuse background is difficult because of the limitations of the γ-ray detection process. Below a few MeV in energy, there is a high background due to continuum emission and nuclear decay line, arising primarily from cosmic ray interactions in and around the detector. Above a few MeV the background is somewhat less, but the photon fluxes are much weaker, still presenting a sizeable signal-to-noise problem.

[1]Also Univ. of Maryland

ORIGINAL PAGE IS
OF POOR QUALITY



Therefore, the key to successful observations of medium energy γ rays is the suppression of instrumental background. A new Compton telescope is being developed at GSFC for point source observations between 1 and 30 MeV. In this instrument, a combination of techniques is used to reduce instrumental background. Furthermore, it is designed to allow accurate subtraction of the residual instrument background as well as the diffuse atmospheric and cosmic fluxes.

## 2. Instrument Description

The telescope, which will be an oriented balloon payload, is shown schematically in Fig. 1. The central detectors are both NaI scintillators, each with 1600 $cm^2$ area; the upper detector, in which the initial Compton scatter of a γ-ray is to occur, is about 2.5 cm thick. The lower detector, in which the scattered gamma ray is absorbed, is about 15 cm in thickness. Each of the two NaI detectors is viewed by a 5 × 5 array of high speed 2" photomultipliers. Signals from these tubes are separately digitized to provide information on the interaction positions within the two detectors, and therefore the trajectory of the scattered γ ray.

The upper NaI detector is sandwiched between two 6 mm sheets of plastic scintillator. A phoswich technique is used to separate the NaI and plastic scintillator signals; the plastic signal is then used as a veto to prevent triggering on events in which a charged particle enters or leaves the upper NaI detector.

The two central detectors are surrounded by a shield of lead, about 5.5 rl thick, which is encased in plastic scintillator anticoincidence counters. These are viewed by an array of 12.6 cm photomultipliers, 12 at the top and 4 at the bottom.

Two techniques are employed to eliminate background from fast neutrons; in each of the central NaI detectors, the pulse shape is determined by direct digitization at a rate of 50-70 MHz. This information is telemetered to the ground for later analysis. The heavily ionizing nuclei resulting from fast neutron interactions produce pulse shapes in NaI which are significantly different from those

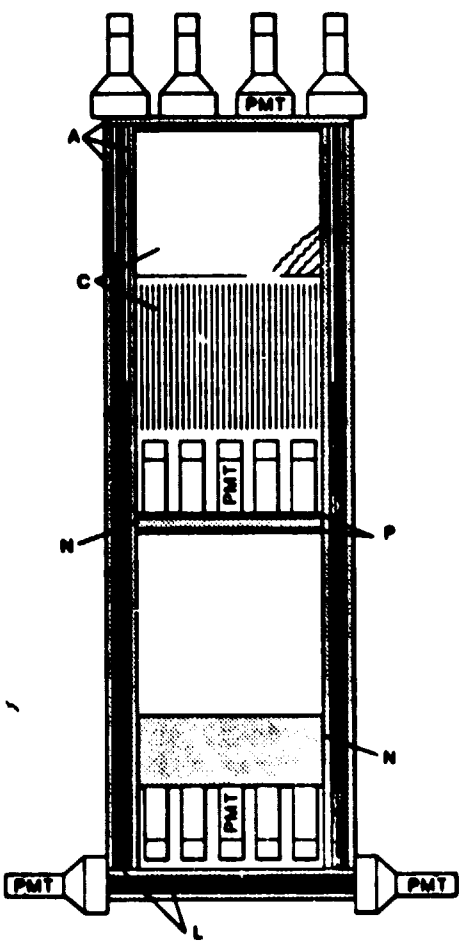


Fig. 1 - Instrument Schematic

N, NaI scintillators; P, phoswich plastic anticoincidence scintillators; A, anticoincidence plastic scintillators; C, lead slot collimator; L, lead shielding

ORIGINAL PAGE IS
OF POOR QUALITY



generated by electrons. The second technique for fast neutron rejection is a time-of-flight measurement between the two NaI detectors. With the 40 cm spacing between these detectors and the relatively slow risetime of the NaI pulse, it probably will not be possible to distinguish between upward and downward moving γ-rays; but it will be possible to separate out and reject those events due to the fast neutrons, which have typical velocities of c/7 or less.

The direction determination is made not by the Anger camera Compton event reconstruction, but by means of two crossed slat lead collimators, giving a field-of-view of about 2°. This permits us to use the Anger reconstruction as a cross-check on the collimator direction. By requiring that the Compton reconstructed direction cone include the collimator direction, it should be possible to reduce by a factor of at least ten the backgrounds due to β-γ decays in the NaI or γ rays originating within the rest of the instrument.

Despite the background elimination precautions mentioned above, some instrumental background will still remain. Furthermore, atmospheric and cosmic diffuse fluxes must be accounted for in the search for localized γ-ray sources. This background subtraction will be accomplished by comparing the rate of acceptable event while pointing on-source to that while pointing off-source. Rather than reorient the entire telescope for this purpose, one of the two slat collimators will be rocked by a few degrees every few minutes. The on-source and off-source positions of the collimator are symmetric with respect to the telescope axis, eliminating any bias due to a changing configuration.

The telescope orientation will be determined and controlled by an on-board closed-loop microprocessor-based system. This system uses as its detector a CID solid state video camera[2] fitted with a 58 mm f/1.2 lens which has extended IR coating. This system has a field-of-view of 8.7° × 11.2°, with angular resolution of 0.045° × 0.036° (244 × 248 pixels). Preliminary tests indicated that this system can detector G-type stars of approximately magnitude 6 with a 5s exposure.

## 3. Conclusions

Based on estimated background as well as increased effective area, it anticipated that, with the instrument described, point source detection sensitivity should be improved by nearly an order of magnitude over earlier balloon instruments.

[2] GE Type TN2500

ORIGINAL PAGE IS
OF POOR QUALITY



# EGRET: THE HIGH ENERGY GAMMA RAY TELESCOPE FOR NASA's GAMMA RAY OBSERVATORY

C.E. Fichtel, D.L. Bertsch, R.C. Hartman, D.A. Kniffen, D.J. Thompson
NASA/Goddard Space Flight Center
Greenbelt, MD 20771 U.S.A.

R. Hofstadter, E.B. Hughes, L.E. Campbell-Finman
Hansen Laboratory, Stanford University
Stanford, CA 94305 U.S.A.

K. Pinkau, H. Mayer-Hasselwander, G. Kanbach, H. Rothermel, M. Sommer
Max-Planck-Institüt für Extraterrestrische Physik
8046 Garching b. München, Federal Republic of Germany

A.J. Favale, E.J. Schneid
Grumman Aerospace Corporation
Bethpage, NY 11714 U.S.A.

## ABSTRACT

The EGRET high energy γ-ray telescope under development for NASA's Gamma Ray Observatory will have an energy range of approximately 12 to 30,000 MeV, energy resolution of about 15% FWHM over most of that range, an effective area of about 2000 $cm^2$ at high energies, and single photon angular accuracy of ~ 2° at 100 MeV, < 0.1° above 5 GeV. This instrument can locate strong sources to an accuracy of about 5 arc min. The instrument utilizes a set of digital spark chambers interleaved with tantalum foils for detection and identification of γ-ray events, and a large NaI(Tℓ) scintillator for energy determination. The system is triggered by a coincidence matrix using two arrays of plastic scintillation counters and a large plastic scintillator anticoincidence dome that rejects incident charged particles.

## 1. Introduction

The Gamma Ray Observatory (GRO), a Shuttle-launched free-flying satellite, is scheduled for launch in the late 1980's. This will be the first mission dedicated to a comprehensive study of the γ-ray portion of the electromagnetic spectrum encompassing over five orders of magnitude in energy. Four instruments will be included to cover the broad range of energies and to achieve the scientific objectives.

The purpose of this paper is to describe the high energy instrument to be included on GRO. This instrument, a spark chamber telescope with a NaI(Tℓ) total energy counter, will cover the energy range from about 12 to 30,000 MeV, with much better sensitivity and spectral and spatial resolution than any previous experiment in this energy range.

## 2. Scientific Objectives

The specific objectives of this experiment are:

- To search for localized γ-ray sources in the energy range from 12 MeV to 30 GeV and to measure their intensity, energy spectrum, position, and possible time variations, including periodic emission

- To improve the knowledge of the locations of known high energy γ-ray sources not identified with objects seen at other frequencies
- To examine supernova remnants and search for evidence of cosmic-ray particle acceleration revealed by high energy γ rays
- To obtain a detailed picture of the diffuse high energy γ-ray emission from the Galaxy which in turn will provide information of fundamental importance in the study of the dynamics of the Galaxy. This should provide a high contrast picture of galactic structure, including spiral arm segments, clouds, the galactic center, and the extended disk (or "halo")
- To determine the relative importance of cosmic ray electrons and cosmic ray nuclei throughout the Galaxy by studying the γ-ray spectrum above 12 MeV and, by combining the results with the continuum radio data, to obtain a better estimate of the galactic magnetic fields
- To detect and examine the high energy γ-ray emission from other galaxies, including both normal galaxies and galaxies which are exceptionally luminous at other wavelengths
- To study the diffuse celestial radiation in the energy range above 12 MeV including its energy spectrum and the degree of uniformity, both on a small scale and a broad scale, measurements of particular importance in relation to several cosmological models
- To search for high energy γ-ray bursts, to study the spectra of low energy γ-ray bursts with high statistical accuracy, and to observe γ-ray lines in solar flares

## 3. Instrument Description

The telescope is shown schematically in Figure 1. A γ ray entering the telescope within the acceptance angle has a reasonable probability of converting into an electron-positron pair in one of the thin Ta foils between the spark chambers in the upper portion of the telescope. If at least one particle of the pair is detected by the directional time-of-flight coincidence system as a downward moving particle and there is no signal in the large anticoincidence scintillator surrounding the upper portion of the telescope, the spark chamber track imaging system is triggered, providing a digital picture of the γ-ray event, and the analysis of the energy signal from the NaI(Tℓ) crystal is initiated. Incident charged particles are rejected by the anticoincidence dome and low energy backward-moving charged particles that do not reach the anticoincidence dome are rejected by the time-of-flight measurement. Events other than the desired γ rays, such as those γ rays interacting in the thin pressure vessel inside the anticoincidence scintillator, are rejected in the subsequent data analysis by inspection of the spark chamber images.

The directional scintillator telescope consists of two levels of a four by four tile array with selected elements in each array in a time-of-flight coincidence. The upper spark chamber assembly consists of 28 spark chamber modules interleaved with 27 0.02 radiation length plates in which the γ ray may convert into an electron pair and in which the interaction point and initial direction of the electrons may be determined. The lower spark chamber assembly, between the two time-of-flight scintillator planes, allows the particle trajectories to be followed, provides further information on the division of energy between the electron and positron, and makes possible the observation of the two particles for very high energy γ rays.

ORIGINAL PAGE IS
OF POOR QUALITY



The energy of the γ ray will be determined primarily from measurements in an eight radiation length, 76 cm × 76 cm square NaI(Tℓ) scintillation crystal below the lower plastic scintillator plane. Below 200 MeV, energy information is also obtained from measurements of multiple scattering in the tantalum foil. The energy resolution of the proposed experiment is better than 15% (FWHM) above 30 MeV.

Gamma-ray bursts will be recorded in both the anticoincidence dome and the large NaI(Tℓ) crystal, where an energy spectrum will also be measured in the 0.3 to 24 MeV interval.

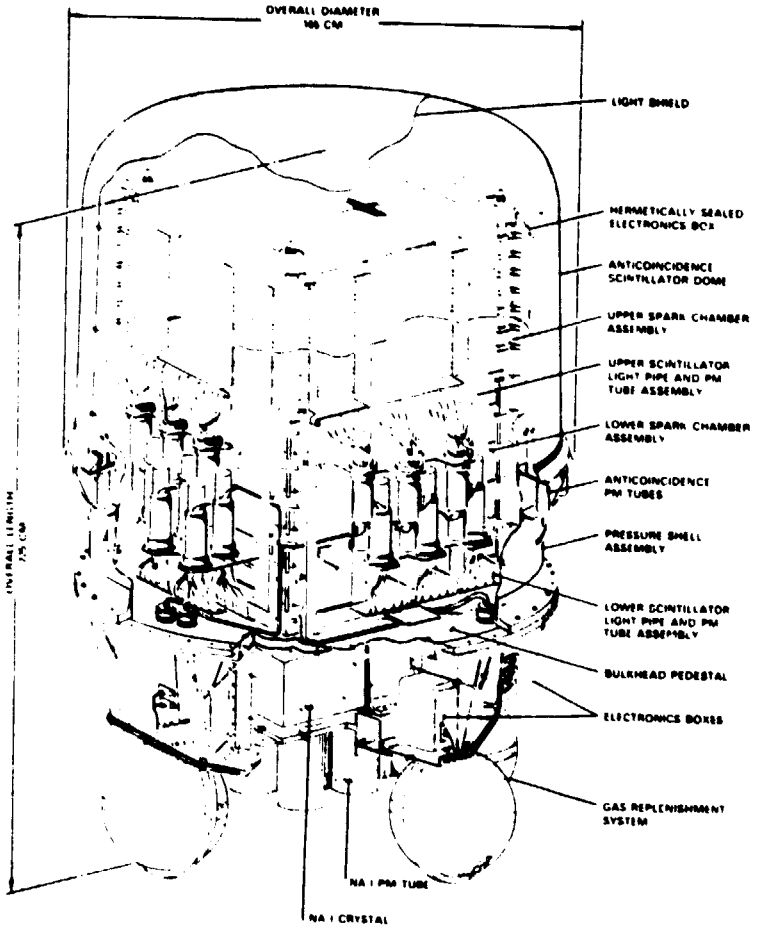


Figure 1: High Energy Gamma-ray Telescope (EGRET)

The principal capabilities of the instrument are summarized in Table 1. For additional details see Hughes et al. (1979).

## 4. Capabilities of the Experiment

The high energy instrument on GRO is characterized by the very low background available with the detection of the pair production interaction. The instrument also has good spectral and spatial resolution and sensitivity which should combine to give this telescope the ability to locate sources with one-tenth the intensity of the Crab pulsar to an accuracy of four to ten arc minutes, depending on the general background level. This gives a factor of well over two orders of magnitude improvement over existing error boxes. The .1 millisecond timing will allow searches for pulsars with periods down to the the 1.5 msec range, provided the period is known.

For the diffuse galactic plane emission, the spectra will be measured with high accuracy, and spatial variations in the spectrum

ORIGINAL PAGE IS
OF POOR QUALITY



Table 1

HIGH ENERGY GAMMA-RAY TELESCOPE
CAPABILITIES AND REQUIREMENTS

| | | |
|---|---|---|
| 1. | Detectors | |
| | a. Type | spark chambers with NaI total energy counter |
| | b. Energy Range | 12 to 30,000 MeV |
| | c. Energy Resolution | 15% 30 MeV - 10,000 MeV |
| | d. Total Detector Area | 6560 $cm^2$ |
| | e. Area Efficiency Factor | 2000 $cm^2$ above about 200 MeV |
| | f. Threshold Point Source Sensitivity ($10^6$ sec) | $5 \times 10^{-8} cm^{-2} s^{-1}$ |
| | g. Angular Resolution | 1.6° at 100 MeV: 0.6° at 500 MeV: 0.2° at 2 GeV (projected rms) |
| | h. Source Resolution (strong source) | 5 arc min |
| | i. Field-of-View | ~.5 sr: maximum opening angle 45° |
| | j. Timing Accuracy | 0.1 ms absolute |
| | k. Design Lifetime | 2 years |
| 2. | GRO-Experiment Interface | |
| | a. Weight | 1830 kg |
| | b. Size | 2.25 m × 1.65 m diameter |
| | c. Power | 180 w including heaters |
| | d. Bit Rate | 6.8 kbps |

should be measurable on a scale of a few degrees. Features which subtend more than about 0.5° will be resolved above 1 GeV as extended sources.

The diffuse radiation away from the galactic plane will be separable into galactic and extragalactic components on a scale of a few degrees. The extragalactic component will be studied for spatial variations in intensity and spectral distribution, providing important clues for determining the origin of this radiation.

With respect to extragalactic discrete objects, the situation is not so easy to predict. The radio galaxy CEN A; two seyfert galaxies, NGC 4151 and MCG8-11-11; and the quasar 3C273 have been seen in γ-rays. The high energy telescope on GRO will have about a ten times lower threshold for the detection of extragalactic objects than COS-B which detected 3C273. If the γ-ray luminosity distribution is similar to that for either x-ray or visible photons, as many as 30 quasars might be expected to be seen. Even pessimistic estimates suggest that at least ten should be seen. Although even more difficult to predict, several normal galaxies should be detectable and for the nearest ones a study of their structure in γ-rays will be possible.

**References**

Hughes, E.B. et al. (1980), IEEE Trans. Nuc. Sci. NS-27, p. 364.

ORIGINAL PAGE IS
OF POOR QUALITY



# A LARGE AREA EXPERIMENT TO DETERMINE COSMIC RAY ISOTOPIC ABUNDANCES

B.G. Mauger*, V.K. Balasubrahmanyan, J.F. Ormes, and R.F. Streitmatter
NASA/Goddard Space Flight Center, Greenbelt, MD 20771, U.S.A.

W. Heinrich, M. Simon, H. O. Tittel
Department of Physics, University of Siegen, 29 Siegen, West Germany

## 1. ABSTRACT

Observations of the cosmic ray isotopes of neon and magnesium have shown an overabundance of the neutron rich isotopes as compared with solar abundances. In order to determine the metalicity of the cosmic ray sources, the isotopic composition of these and other fluxes must be studied. A 1.2 $m^2$-sr instrument to study the isotopic composition of the elements from oxygen through argon is being constructed as a joint project between the University of Siegen, West Germany and the Goddard Space Flight Center, U.S.A. This instrument uses two scintillators and two Cherenkov detectors (n = 1.33 and 1.4). Each of these radiators must have a uniform response to within 1 percent in order to achieve a mass resolution of .3 amu. To achieve this uniformity of response, each radiator will be frosted to eliminate specular reflections and will be used to determine the trajectory within ± 1 mm. A passive nitrocellulose range stack determines the range of the particles. These sheets of nitrocellulose are etched in an ammonia bath and the position of the tracks are read by computerized scanning. It is expected that this experiment will be able to determine the isotopic abundances in the energy range of 300 to 800 MeV/nucleon for elements from oxygen through argon.

## 1. INTRODUCTION

Experiments to measure the isotopic composition of cosmic rays have shown an enrichment of neutron rich isotopes as compared with solar abundances. The cosmic ray isotope ratios, $^{22}Ne/^{20}Ne$ and $(^{25}Mg + {}^{26}Mg)/^{24}Mg$, exceed the solar abundance ratios by factors of 2.7 and 1.8, respectively (Fisher et al., 1976; Greiner et al., 1979; Mewalt et al., 1980).

There are several processes that could be responsible for the excess of these neutron rich isotopes. (For a discussion, see Woosley and Weaver, 1981.) The implications of these models also predict various amounts of neutron enrichment of other, less abundant, species. If measured, these isotopic abundances could determine which processes dominate in cosmic ray sources. In order to measure the isotopic abundances of these species, a large area experiment with a mass resolution of better than .3 amu is necessary.

NAS/NRC Research Associate

ORIGINAL PAGE IS
OF POOR QUALITY



Such an experiment is under construction as a joint effort between the University of Siegen, West Germany and NASA's Goddard Space Flight Center. This experiment, the Aluminum Isotopic Composition Experiment (ALICE), uses a Cherenkov-range technique to determine isotopic composition of elements from oxygen through argon. The experiment has a geometry factor of 1.2 $m^2$ st and uses two Cherenkov detectors to increase its dynamic range.

## II. DETECTOR COMPLEMENT

Figure 1 schematically shows the detector complement. Two scintillators, S1 and S2, form a coincidence telescope to define an event. These scintillators are 120 cm x 120 cm x 1 cm Polycast "PS-10" scintillators. In order to provide a uniform response, the surfaces of these scintillators are frosted (to eliminate specular reflections), housed in diffusive light collection boxes, and viewed by 16 12.5 cm photomultiplier tubes. The interior of the light collection boxes is painted with a barium sulfate paint with a .95 reflectivity. The light collection efficiency of these boxes is on the order of 50 percent.

The trajectory of the cosmic ray is determined by the drift chambers, DCI and DCII. Prototype drift chambers have been tested in the heavy ion beam at Berkeley (Simon et al., 1981). These chambers should provide sufficient spatial resolution to trace the cosmic ray through the detector stack to ± 1 mm.

The two Chereknov detectors CI and CII, are housed in light diffusion boxes identical to those containing the scintillators. Because Chereknov detectors are most sensitive near threshold, two Cherenkov detectors with different indices of refraction are used. CI is a 2 cm thick piece of Pilot 425 with a refractive index of 1.33. CII is a silicon based rubber, GE RTV-615, with a refractive index of 1.4.

Below DCII is a passive range stack of cellulose nitrate, CN. The range stack has a depth of 15 g/$cm^2$ (11 cm) made of .03 g/$cm^2$ (250μm) foils. After the flight, these foils will be etched and the resultant tracks transferred to a print by an ammonia scan method. These prints will then be digitized by a computerized scanning microscope.

At the bottom of the range stack, there is an anticoincidence scintillator, ANTI, which is used to reject particles which are not stopped by the range stack.

## III. MASS RESOLUTION

In order to achieve a mass resolution of better than .3 amu, it is necessary to determine the range and the energy per nucleon (from the Chereknov detectors) to within 1 percent. One source of range error is struggling, which cannot be reduced by experimental methods. Another source of range error occurs due to uncertainties in the amount of material between the velocity (Cherenkov) measurement and the range stack. Special design consideration has been given to the construction

ORIGINAL PAGE IS
OF POOR QUALITY

of the light diffusion boxes and the drift chambers to keep mass uncertainties below a few hundredths of a $g/cm^2$.

Errors in the velocity measurement can occur for a variety of reasons. To eliminate variations in the Chereknov response, the double-diffuse light gathering technique described above is used.

To remove any residual response nonuniformities, the detectors will be response-mapped using relativistic particles before and during the flight. With a mapped response profile, the uniformities of the detectors should be reduced to below 1 percent. Since the photo cathodes represent a small fraction of the diffusion box's area, on the average, each photon suffers many diffuse reflections before being detected. Finally photon counting statistics limit the accuracy of the Cherenkov detectors. Figure 2 shows the estimated mass resolution of the instrument.

## References

Fisher, A. J., Hager, F. A., Maehl, R. L., Ormes, J. R., and Arens, J. F. 1976, Ap. J., 205, 938.

Greiner, D. E., Wiedenbeck, M. E., Bieser, F. S., Crawford, H. J., Heckman, H. H., and Lindstrom, P. J. 1979, Proc. 16th Int. Conf. Cosmic Rays, 1, 418.

Mewalt, R. A., Spalding, J. D., Stone, E. C., and Vogt, R. E. 1980 Ap. J. Lett., 235, L95.

Simon M., Henkel, M., Schieweck, G. 1982, NIM, 192, 483-489.

ORIGINAL PAGE IS
OF POOR QUALITY



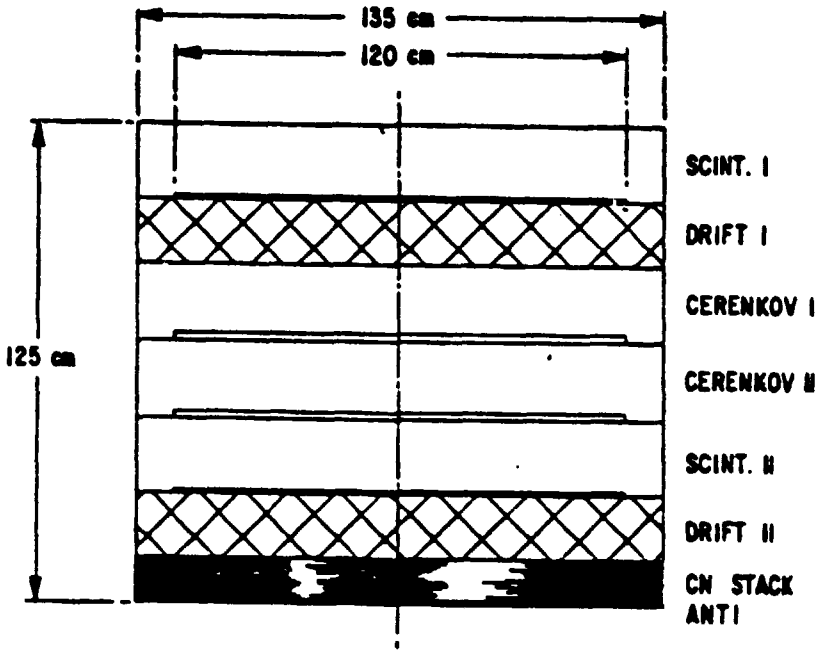


Figure 1. The ALICE detector complement

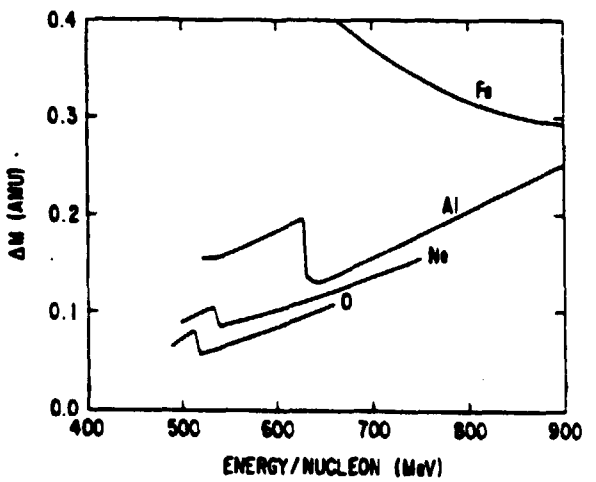


Figure 2. Predicted ALICE resolution.

ORIGINAL PAGE IS
OF POOR QUALITY



# A METHOD TO DETECT ULTRA HIGH ENERGY ELECTRONS USING EARTH'S MAGNETIC FIELD AS A RADIATOR

S. A. Stephens* and V. K. Balasubrahmanyan
NASA/Goddard Space Flight Center, Greenbelt, MD 20771

## 1. INTRODUCTION

Detection of high energy electrons above a few TeV, which lose energy rapidly through synchrotron and inverse Compton processes, would give valuable information on the distribution of sources and on the propagation of cosmic rays in the solar neighborhood. The influence of a strong nearby source would also be seen as a marked enhancement over the depleted electron spectrum. However, none of the existing experimental techniques could be used to measure the energy spectrum beyond a few TeV. We examine here the possibility of detecting electrons [1] above a few TeV by the photons emitted through synchrotron radiation in the Earth's magnetic field. As these photons are emitted in the direction of the electron within an extremely narrow cone, they would be incident on a detector almost along a straight line. This pattern provides an unique signature for the identification of the electron. The mean energy of the emitted photons, being proportional to the square of the energy, provides reliability in the energy estimation even if a detector has low energy resolution. Thus, this technique would open up an important window of energy for the study of primary cosmic ray electrons.

## 2. SYNCHROTRON RADIATION OF ELECTRONS IN EARTH'S MAGNETIC FIELD

The theory of synchrotron radiation is extensively discussed in the literature [2]. The spectral shape of photons emitted by an electron has a slope of -2/3 at low energies, slowly steepens at higher energies, and drops off exponetially beyond $E_c = 6.56 \times 10^{-2} B_\perp E_o^2$ MeV; $B_\perp$ in Gauss and $E_o$ in TeV. It can be shown that 70 percent of the photons emitted are spread over 2 decades in energy. The mean energy of the photons is proportional to the square of the electron energy, and in order to cover m decades of electron energy, one needs an instrument capable of detecting photons over $(m^2 + 2)$ decades in energy.

Photons are emitted within a narrow cone in the direction of electrons. The radiation is polarized, and the angular distributions of photons along the two principal directions of polarization are different. We infer from the angular distribution of photons that 70 percent of the photons are emitted within $0.65 \times 10^{-7}$ radian. This correspond to a spread of only 1.3 cms on to a detector placed at a distance of 100 km, implying that the photons are distributed approximately along a straight line.

With a typical balloon altitude corresponding to a depth of $4\ g\ cm^{-2}$ of atmosphere over Palestine, Texas as the initial point on the trajectory of the electron, we have traced its trajectory in Earth's field using sixth degree simulation of the geomagnetic field [3,4]. Figure 1a shows an exaggerated view of the trajectory of an electron.

ORIGINAL PAGE IS
OF POOR QUALITY



In this figure O is the arrival point, B's denote the steps with step length $\Delta s$, and A's are the intercepts on the detector plane by tangents $B_1A_1$, $B_2A_2$,... at point B's on the trajectory. The wavy lines are indicative of the photons emitted by the electron. At each step, we have calculated the new coordinates, $B_i$, the radius of curvature, the distance swept by the tangent $\Delta\ell$, and $\ell = \sum \Delta\ell$. The energy spectrum of photons > 20 keV is corrected for the absorption of photons in the air between the detector and the point of emission. The total number of photons received over $\Delta\ell$, the energy flow, the mean energy $\langle E_\gamma \rangle$, and their angular distribution are determined.

## 3. DETECTOR RESPONSE AND ENERGY ESTIMATION

When an electron passes through the detector, the photons would be incident only on the convex side of the trajectory (Fig. 1a). This is a special situation making the identification of the electron event very unique. Even if the electron does not intercept the detector, one can still identify the electron by the colinearity of the incident photons. The number of photons required to identify an event unambiguously is $n_\gamma > 3$. We have calculated the response area $A_R$ of a detector using this criterion. We divide the detector into a number of strips (Fig. 1b) of width $\Delta b$ parallel to the arrival direction. If the electron arrives at O, the detector strip would have 3 photons (filled circles) between O and D, and none between O and A. Therefore, the minimum length required by the detector is OD = $\ell$. As the electron moves towards A, the number of photons detected increases, reaching a maximum at A, and then decreases to less than 3 photons beyond O. Thus, the maximum distance up to which an electron can be detected is O'D = $\ell 2$. The response area of the strip is $(\ell_2 - \ell_1) \times \Delta b$.

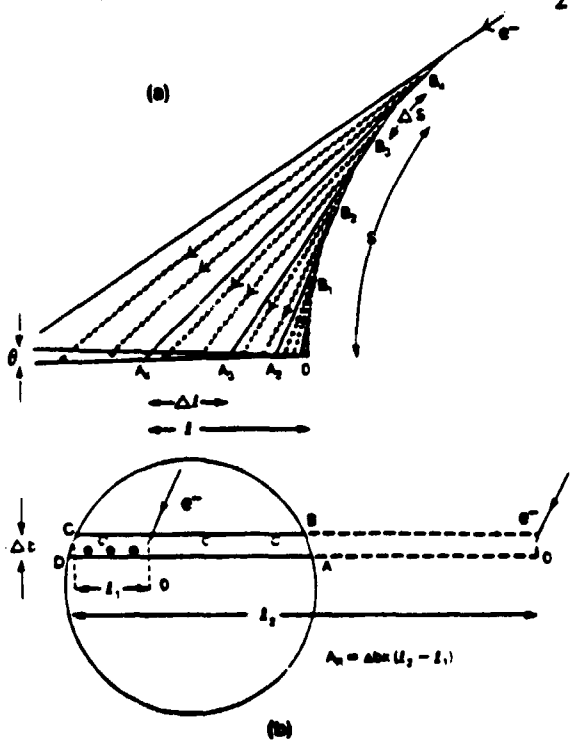


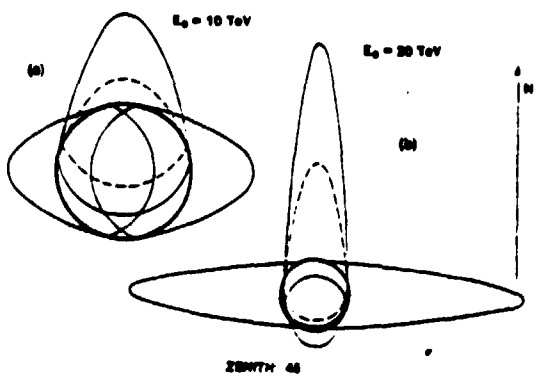


Fig. 2 (above)--The response pattern

Fig. 1 (left)--A schematic diagram

The calculated response of a circular detector is shown in Fig. 2 for electrons arriving at a zenith angle of 45°. The detector is shown by thick circles. The thin curves trace the circumference of the response area for $n_\gamma = 5$. The effect of increasing the value of $n_\gamma$ to 7 photons is shown by the dashed curve for North. The dramatic increase of the response area with $E_o$ can be noticed from this figure at 20 TeV; this figure is scaled down by a factor of 2. The response area (a) varies with the arrival direction of electrons, (b) appears elongated along the diameter, indicating its dependence on the shape and size of the detector, (c) decreases as the value of $n_\gamma$ is increased, and (d) increases with energy.

Knowing $B_\perp$, the energy of an electron can be determined from the observed mean energy of photons. Since, the number of particles detected by an instrument in a direction $(Z, \phi)$ is proportional to the collecting power $CP(Z,\phi)$ in that direction, one can make use of the calculated CP to draw histograms of the estimated $\langle E_\gamma \rangle$. CP is the product of the projected $A_R$ perpendicular to the arrival direction, and the solid angle is that direction. Using this, we examine the viability of using an omnidirectional detector to study electrons. Fig. 3 shows histograms of $\langle E_\gamma \rangle$ using an omnidirectional detector of radius 150 cms for $E_o = 10$ TeV and $n_\gamma = 5$ photons, with zenith angle cuts as indicated. The peak in the distribution shifts to higher energies as one includes larger zenith angles, because of the higher mean $B_\perp$. It can be shown that $\langle E_\gamma \rangle$ distribution is independent of $n_\gamma$ and the detector area. The distributions are asymmetric. The half widths at half maximum, in terms of the energy of the electron, are about 15 and 5 percent of the peak value towards lower and higher energies. For a typical experiment discussed here, we obtain a relation for the most probable energy as $\langle E_\gamma \rangle_m = 0.0225\ E_o^{1.76}$ MeV. It may be noted that this relation is based on the assumption that the instrument has 100 percent detection efficiency for photons > 20 keV. In actual practice this is not true, and one needs to include both the detector efficiency and the energy response to obtain a similar relation.

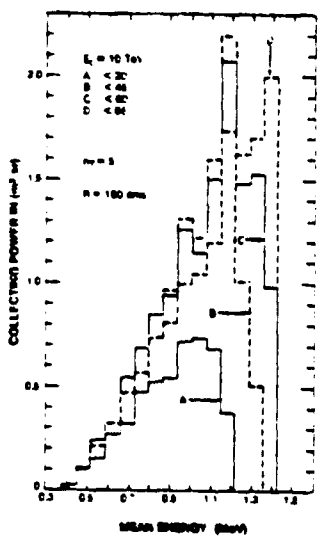

Fig. 3 Histograms of $\langle E_\gamma \rangle$

## 4. DETECTION OF ELECTRONS

We have calculated the collecting power of an omnidirectional detector and examined its dependence on $E_o$, the area of the detector, and the selection criterion $n_\gamma$. It is found that as long as A is not very small and $n_\gamma$ not very large, the collecting power of a detector is asymptotically proportional to $A^\alpha E_o n_\gamma^\beta$, where $\alpha = 1.43$ and $\beta = -1.8$. As the energy decreases, CP deviates fr[illegible] its linear dependence on $E_o$ and decreases by an order of magnitude [illegible] a decrease of energy by a factor

of 2. This behavior provides the threshold detection for electrons, and thus, the integral flux can be determined accurately even by an instrument with limited energy resolution.

For an ideal detector, capable of detecting photons > 20 keV, we have calculated the expected rate of electron events using an electron spectrum of the type $j(E_o) = 500\ E_o^{-3.2}$ electrons/($m^2$ sr s GeV). The event rate thus calculated is shown in Fig. 4 as a function of the energy of electron for various values of $n_\gamma$ and A. Curves A, B, and C in this figure correspond to circular detectors with radii 200 cms, 100 cms, and 50 cms, respectively. The collection time in a typical balloon flight is about 20 hours. Using a detector of area $10m^2$, a total of about 13 electrons can be observed at energies above 5 TeV using $n_\gamma$ criterion of 4 photons; this number reduces to about 8.5 for $n_\gamma = 5$ photons. From a 14-day space shuttle flight one can collect about 100 events above 5 TeV and about 3 events above $10^{14}$ eV. As there is no atmospheric absorption of X-rays, the detection threshold is decreased and the number of events would be larger. We have compared these event rates with that expected from a proposed [5] shuttle experiment as shown by the curve TRIC; the expected number of events is only 0.5 electron above 5 TeV.

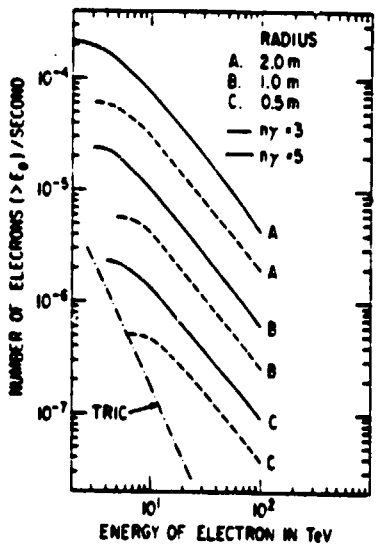


Fig. 4. Expected event rate

## REFERENCES

[1] Stephens, S. A. and V. K. Balasubrahmanyan, submitted to JGR, 1983.
[2] Ginzburg, V. L. and Syrovatskii, Ann. Rev. Astr. Ap. 3, 297, 1965.
[3] McCraken, K. A., et al., M.I.T. Technical Report 77, 1962.
[4] Daniel, R. R. and S. A. Stephens, Proc. Ind. Acad. Sci., 63, 275, 1966.
[5] Ormes, J. F., Proc. 'Workshop on high energy cosmic ray interactions', Philadelphia, p 466, 1982.

*NAS/NRC Senior Research Associate on leave from TIFR, Bombay